

**Mold, Flow, and Economic Considerations in High Temperature
Precision Casting**

By

Matthew S Humbert

B.S. Mechanical Engineering
Massachusetts Institute of Technology, 2008

SUBMITTED TO THE DEPARTMENT OF MATERIALS SCIENCE AND
ENGINEERING IN PARTIAL FULFILLMENT OF THE REQUIREMENTS FOR THE
DEGREE OF

MASTER OF SCIENCE IN MATERIALS SCIENCE AND ENGINEERING
AT THE
MASSACHUSETTS INSTITUTE OF TECHNOLOGY

JUNE 2013

©2013 Massachusetts Institute of Technology. All rights reserved.

Signature of Author: _____
Department of Materials Science and Engineering
May 1, 2013

Certified by: _____
Thomas W. Eagar
Professor of Materials Science and Engineering & Engineering Systems Division
Thesis Supervisor

Accepted by: _____
Gerbrand Ceder
Chair, Departmental Committee for Graduate Students

Acknowledgements

1. Industrial Partners
 - a. Tiffany & Co. Jewelers – Primary funding
 - b. Almatis Premium Alumina – Alumina products
 - c. Allied Minerals – Spinel and other refractory
 - d. Remet Corp – Casting and slurry advice
 - e. Niobec – Ferro Niobium
2. MIT support
 - a. Faculty and Staff
 - i. Thomas Eagar –Advisor and all that entails
 - ii. Mike Tarkanian – For providing space and encouragement
 - iii. Harold Larson, Don Gallar, David Bono – For technical support
 - iv. Chris, Ike, and Franklin – For taking over my old job
 - v. Angelita, Elissa, Julia –For keeping the administration off my back
 - b. Co-workers
 - i. Alan, Zack, Sam, Steve, Nihan – Where would I be without helping you with your research?
 - ii. Guillaume, Brice, Antoine, and Sal – The group I wasn't in
 - c. Coffee hour – For making MIT bearable
 - d. UROPs
 - i. Yvonne S., Celine Y., Mike G., Tobi A., James M. – I couldn't have done this without you.
3. Family
 - a. Mom – For telling me to relax
 - b. Dad and Susan – For always giving me a place to hide
 - c. Marc – For never being afraid to talk shop
4. The MechE guys
 - a. Wayne, Kevin, Dan, Joe, Joe – Thanks for keeping it real
5. The rest of the people I know
 - a. Colin, Dina, Orian, Claire, Karen, Dan, Sharms, Billy, Maria, Patrick, Doug, Jim, Jim, James, Amanda, Chris Emma, Madeline, Jen, Ian, Ellen and everyone else – Time to have fun again!
6. My best friend Erik – Through it all

Mold, Flow, and Economic Considerations in High Temperature Precision Casting

By

Matthew S. Humbert

Submitted to the Department of Materials Science and Engineering
on May 1, 2013 in Partial Fulfillment of the
Requirements for the Degree of Master of Science in
Materials Science and Engineering

ABSTRACT

Casting high temperature alloys that solidify through a noticeable two phase region, specifically platinum-ruthenium alloys, is a particularly challenging task due to their high melting temperature and this necessitates careful design of the mold material and mold geometry to produce defect free castings. Here fluid flow, heat flow, and chemical interactions were investigated with simulations and casting experiments. Three mold recipes were developed; an improved magnesium-phosphate binder silica sand based system, a magnesium-aluminum phosphate binder alumina sand based system, and a colloidal zirconia sol binder zirconia sand based system. The fluid and heat flow analysis has shown, and has been verified by experiment, that using a mold material with a low heat diffusivity, (the product of thermal conductivity, heat capacity, and density) will improve casting quality by delaying solidification and reducing interdendritic porosity. A simple economic framework was developed to compare the price of different ceramics with the results showing that silica is a more economic mold material at an estimated 75% yield over a zirconia or alumina mold with a 100% yield. This framework neglected how secondary processing and efficiency gains affect cost. The likely implementation of this research will be a zirconia face coat supported in the flask by magnesium phosphate bonded silica. This will provide the required heat diffusivity and mechanical support at the lowest cost to minimize interdendritic porosity.

Thesis Supervisor: Thomas W. Eagar

Title: Professor of Materials Science and Engineering & Engineering Systems Division

Table of Contents

Abstract.....	3
List of Figures	6
List of Tables.....	8
1. Introduction.....	9
1.1 Motivation	9
1.2 Simplifying Assumptions.....	10
1.3 Concepts and Variables	11
2. Fluid Flow.....	13
2.1 General Considerations of Fluid Flow	13
2.2 Filling vs Feeding.....	16
2.3 Flow Simulation	19
3. Heat Flow	21
3.1 General Considerations of Heat Flow	21
4. Mold Ceramic	24
4.1 General Considerations for Mold Ceramics.....	24
4.2 Toxicity	24
4.3 Thermochemical Stability & Melting Point.....	24
4.4 Mechanical Durability.....	27
4.5 Making A Slurry.....	27
4.6 Binding the Ceramic.....	28
5. Cost Model.....	30
5.1 Profit, Yield, Price and Cost	30

5.2	Justifying A Higher Cost Ceramic	31
6.	Methods.....	33
6.1	Overview of Methods.....	33
6.2	Ceramic Testing Scheme.....	33
7.	Results and Observations	35
7.1	Molds.....	35
7.1.1	Ceramic Recipes	35
7.1.2	Firing Schedules.....	37
7.1.3	Mold Material Tests	37
7.1.4	Other Mold Considerations.....	39
7.2	Fluid Simulation Results	39
7.2.1	Simulation Workflow.....	39
7.2.2	Single Ring Filling.....	40
7.2.3	Effect of a Screen.....	41
7.2.4	Effect of a Conical Diffuser.....	42
7.2.5	Final Design and Benchmark.....	42
7.3	Casting Results.....	44
8.	Conclusions from Results and Future Work.....	45
8.1	Fluid Flow	45
8.2	Heat Flow	45
8.3	Mold Ceramic and Economics	45
9.	References.....	46
10.	Appendix A – Using Blender.....	48
11.	Appendix B – Data on ceramic compositions.....	53
12.	Appendix C – Index to Fluid Simulation Results	57

List of Figures

FIGURE 1: TWO DIFFERENT SURFACE PORES. PORE “A” RESULTED FROM AN ENTRAINED GAS BUBBLE THAT FAILED TO FULLY COLLAPSE, WHILE “B” RESULTED FROM SOLIDIFICATION SHRINKAGE.	10
FIGURE 2: ILLUSTRATING HOW THREE PHYSICAL CONCEPTS REDUCE TO FOUR PROCESSING VARIABLES.....	12
FIGURE 3: AS CAN BE SEEN FROM ABOVE, PER UNIT LENGTH INTO THE PAGE, A DECREASE IN THE AREA TO PERIMETER RATIO REQUIRES AN INCREASE IN SUPER HEAT TO MAINTAIN THE SAME SOLIDIFICATION TIME. THE RATIO OF ENTHALPY OF FUSION TO SPECIFIC HEAT IS ESTIMATED AT 1000:1 BASED ON DATA TAKEN FROM SMITHELLS AND IS RELATIVELY CONSTANT FOR METALS.....	15
FIGURE 4: BOTH CROSS SECTIONS HAVE THE SAME AREA, BUT TURBULENCE WAS NOTABLY REDUCED WITH THE CRUCIFORM FLOW GEOMETRY.	16
FIGURE 5: CAMPBELL’S ILLUSTRATION OF FEEDING MECHANISMS. SEE HIS WORK FOR A MORE COMPLETE DISCUSSION ON FEEDING.....	17
FIGURE 6: DENDRITIC SOLIDIFICATION STRUCTURE OF THE PT-5%RU ALLOY FROM (FRYE AND FISCHER-BUEHNER)CIRCLE INDICATE PORES THAT HAVE FORMED EITHER AT GAIN BOUNDARIES OR IN BETWEEN DENDRITE ARMS.	18
FIGURE 7: SOME PRELIMINARY VISUALIZATIONS TO LOOK AT SPLASHING AND JETTING IN THE RIGGING. ENTRAINMENT CAN BE SEEN IN THE POURING CUPS OF THE CENTER AND RIGHT IMAGES.....	20
FIGURE 8: THE IMAGE ON THE LEFT HAS BEEN GENERATED BY BLENDER WHILE THE IMAGE ON THE RIGHT WAS CAPTURED WITH A HIGH SPEED CAMERA.....	20
FIGURE 9: FOR THREE DIFFERENT CERAMICS, SILICA, ALUMINA, AND ZIRCONIA SUPERHEAT IS PLOTTED AGAINST SOLIDIFICATION TIME. THE GEOMETRY USED TO PRODUCE THIS PLOT WAS A CIRCULAR PIPE WITH A ONE MILLIMETER RADIUS. TABLE 1 BELOW LISTS THERMODYNAMIC VALUES FOR THE CERAMIC MATERIALS.....	23

FIGURE 10: ILLUSTRATION OF THE TESTING AND ITERATION PROCESS USED TO EVALUATE CHANGES IN THE CASTING PROCESS.	34
FIGURE 11: MOR OF THE UNFIRED MOST PROMISING CERAMICS.....	38
FIGURE 12: MOR OF THE FIRED MOST PROMISING CERAMICS.	38
FIGURE 13: THE FLUID SIMULATION DESIGN PROCESS.....	40
FIGURE 14: A REPRESENTATIVE SELECTION OF SOME INITIAL DESIGNS.	40
FIGURE 15: THE IMAGE ON THE LEFT SHOWS HOW THE SCREEN IS ORIENTED WHILE THE IMAGE ON THE RIGHT SHOWS THE SMOOTH FILLING OF THE CAVITY.....	41
FIGURE 16: THE IMAGE ON THE LEFT SHOWS TURBULENCE ENTERING INTO THE PART CAVITY WHILE THE FIGURE ON THE RIGHT SHOWS A SMOOTH FLUID FRONT PROGRESSING UP THE GATE.....	42
FIGURE 17: A SIDE BY SIDE COMPARISON OF EIGHT FRAMES OF THE REDESIGNED SPRUE (LEFT) AND THE “BUTTON” DESIGN (RIGHT). FRAMES ARE SHOWN AT THE SAME TIME SO TURBULENCE CAN BE COMPARED. THE TOTAL ELAPSED TIME FROM TOP TO BOTTOM IS ~0.29 SECONDS.....	43
FIGURE 18: CASTING RESULTS; (A) SHOWS A PORE THAT FORMED IN THE IMPROVED GEOMETRY SILICA MOLD, (B) SHOWS A PORE THAT FORMED IN THE ALUMINA MOLD, (C) SHOWS A PORE THAT FORMED IN THE ZIRCONIA MOLD. THE SECOND LINE REFLECTS THE SAME PORES AT HIGH MAGNIFICATION.	44

List of Tables

TABLE 1: COMPILED PHYSICAL PROPERTIES OF OXIDES THAT CAN BE USED AS MOLD MATERIALS FOR PLATINUM CASTING.....	26
TABLE 2: THE pH OF MAXIMUM POSITIVE ZETA POTENTIAL IS DEPENDENT ON THE METAL OXIDE ACID-BASE CHARACTER.(CARNIGILA AND BARNA).....	28
TABLE 3: SOME SYSTEMS AND THEIR ASSOCIATED COST PER VOLUME.....	31
TABLE 4: THE MOST PROMISING SILICA BASED MOLD SYSTEM RECIPE.	35
TABLE 5: THE ORIGINAL SILICA RECIPE AS SUPPLIED FROM THE MANUFACTURER (LANE INDUSTRIES)	36
TABLE 6: RECIPE FOR ALUMINA BASED MOLD MATERIAL.....	36
TABLE 7: RECIPE FOR ZIRCONIA BASED MOLD MATERIAL..	37

1. Introduction

Successful castings are dimensionally accurate and mechanically sound. This means that there will be no defects such as porosity, finning, cold shuts, scaling, thermal warping, shrinkage, or any number of engineering terms that require additional processing or warrant remanufacture. There is an enormous amount of literature on casting defects and as such they will be discussed in detail here only as specifically needed. For more information the reader is referenced to the ASM Handbook on Casting, the AFS volume “Analysis of Casting Defects”, and Campbell’s work, “The Casting Handbook”.

This discussion will focus specifically on the platinum 5% ruthenium alloy commonly used for jewelry due to its high luster and hardness. This alloy is commonly flask cast using a centrifugal casting machine. A centrifuge introduces the metal into the mold faster than would be possible by gravity and reduces the riser head needed to fill fine features, (filigree). Though flask casting is a different technique than shell casting, (used primarily for super alloys) much of the discussion results summarized here can generally be applied to both investment casting processes.

1.1 Motivation

The most common defects found in platinum castings are on the surface, and because cast platinum is primarily used for jewelry, these are the principle concern for quality. Some defects are small enough that they can be repaired by laser welding, but this is costly and time consuming. Additionally, these defects can be small enough to pass initial inspection and not be detected until later finishing steps. This further increases the cost of repair and demands sound initial castings. Figure 1 shows two SEM images of surface defects found in a ring.

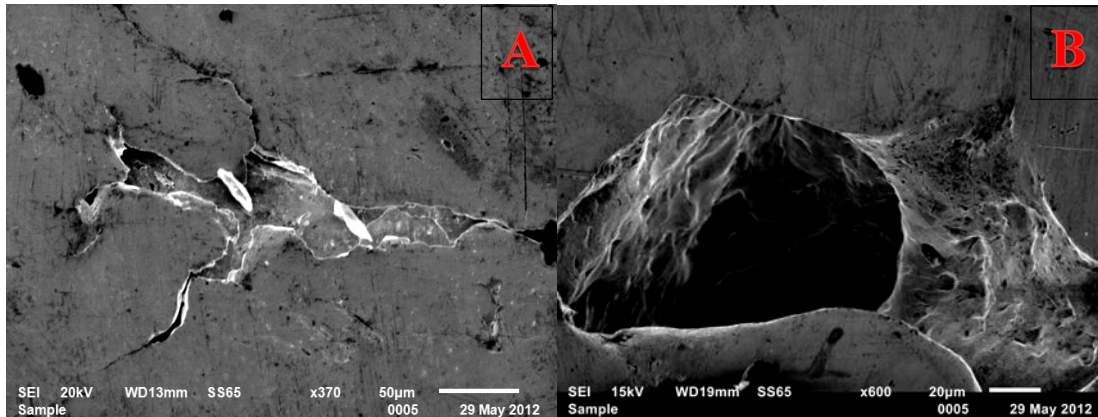


Figure 1: Two different surface pores. Pore “A” resulted from an entrained gas bubble that failed to fully collapse, while “B” resulted from solidification shrinkage.

The defect in Figure 1A was determined to be a cold shut by observing the thin “tails” radiating from the center. The pore in Figure 1B most likely formed as a result of solidification shrinkage. The smaller pores on the inside walls and smooth irregular surface support this.

Looking at other alloy systems, IN713C also suffers from defects that are similar to those observed in platinum. Matysiak et. al.(1)

(1) have compiled a terse overview of common defects found in the IN713C alloy after casting, though they do not report on solutions. Their observations support the hypothesis about the formation of the defects observed in platinum.

1.2 Simplifying Assumptions

Assuming the geometry and alloy are fixed by extraneous conditions, (aesthetic design and metallic luster for jewelry), the foundry is left to optimize the casting process. To do this three things need to be considered; heat transfer, chemical interactions, and fluid flow. These three phenomena are coupled, but with a few observations the design process becomes tractable and the process variables reduce to; casting temperature, mold temperature, mold composition, and fluid flow path. The simplifying assumptions made are:

- The metal quality is consistent
- No metal-atmosphere reactions
- Minimal dissolved gas - Porosity does not vary with atmosphere

The assumption that the metal is consistently pure has been verified by inductively coupled plasma mass spectroscopy (ICP-MS). Several lots of metal were tested and the

composition was not found to correlate with parts rejected for defects. Both scrap and virgin metal were tested from an industrial partner. Were the quality and purity of the metal correlated with the observed defects, an additional variable would need to be considered. Since no correlation was observed it can be concluded that any impurities or defects found in the final casting must be a result of improper or uncontrolled processing in the foundry.

The second observation is that the casting atmosphere is controlled by evacuating the casting machine. Though there is negligible thermodynamic driving force for the absorption of atmospheric gases (N₂, CO₂, O₂, and H₂) controlling the atmosphere removes this possibility entirely. Platinum and ruthenium have no stable, non-volatile oxides, nitrides, or hydrides at the casting temperature, and thus should not contain dissolved gas from these reactions. Oxides, nitrides, and hydrides may appear at temperatures well above the casting temperature, but because they are gas species they should be carried away during filling. The formation rates of these compounds are very slow and can be disregarded during casting operations. (2)

Platinum does have a strong affinity for carbon (3), though it has been discounted as a possible contaminate. Residual carbon left on the surface of the platinum as grease and oil from cutting operations has not been considered an issue because it should volatilize or combust into CO₂ long before absorption into the platinum bulk becomes possible. From Ferguson, carbon will not have an appreciable diffusion rate into platinum at temperatures below ~900C at which point residual hydrocarbons should not be present.

Though platinum alloys don't display the affinity for gas species that other alloys do there is a tendency for a fluid to contain small amounts of dissolved gas. Sieverts' law states that the concentration of a gas dissolved in a metal is proportional to the partial pressure of that gas in the atmosphere. By casting the same alloy under both vacuum and natural atmospheres the amount of dissolved gas can be assessed. This is referred to as a variable pressure, reduced pressure, or Straube-Pfeiffer test. This is a common test performed primarily in aluminum foundries to determine the amount of dissolved hydrogen. Further reading is available in the ASM Handbook Vol 15: Casting. A qualitative comparison between porosity observed in alloys cast in air (4), and those cast under vacuum in the lab show negligible difference in the size, morphology, or concentration of porosity. This observation shows that porosity in platinum alloys is not a result of gas coming out of solution, which again reduces the number of variables that need to be considered.

1.3 Concepts and Variables

From inspection there are three concepts the casting engineer must consider when assessing the casting process; heat transfer, fluid flow, and chemical reactions. From these three concepts, and the above assumptions, four primary variables arise; mold temperature, metal casting temperature, mold properties, and flow design. Figure 2 illustrates this concept.

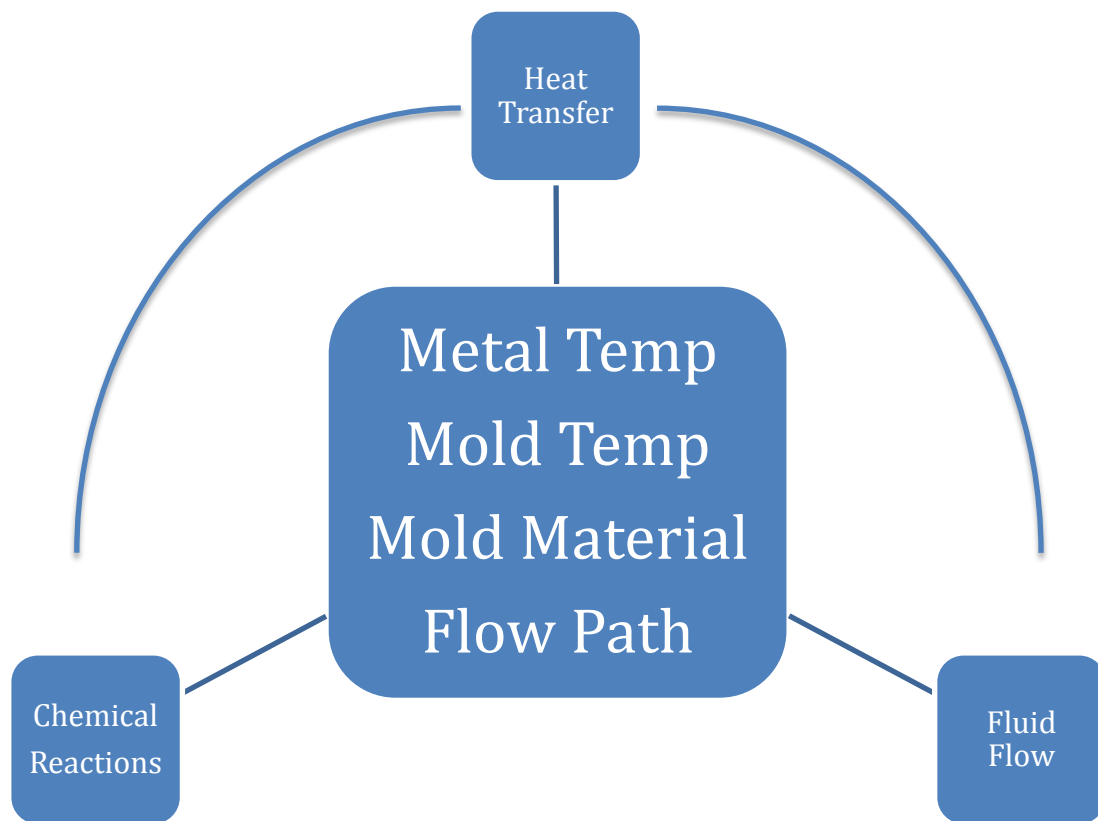


Figure 2: Illustrating how three physical concepts reduce to four processing variables

Within the design landscape formed from these four variables the casting engineer must find the optimum balance that results in the highest casting yield. This work will explore the relationship between these variables.

2. Fluid Flow

2.1 General Considerations of Fluid Flow

Designing the rigging, the flow system surrounding the part, is the most challenging and crucial part of the casting process. The governing equations of fluid flow have limited predictive power to aid the design process and as such rigging systems often rely on empirical iterative experience. This experience is slowly being justified by clever experiments, but is still far from completely characterizing the physics involved. The installation of liquid metal into a cavity involves the displacement of air or mold gas, (even under very good vacuum), and this constitutes a multi-phase flow with a turbulent free surface, one of the hardest to accurately model. Aspects of flow considered here include:

- Assessment of compressibility
- The effect of surface tension, acoustic impedance, and viscosity
- The evaluation of the Weber and Reynolds numbers
- Maintaining flow rate while reducing hydraulic diameter
- The relationship between geometry and solidification
- Computer simulation

A discussion of fluid flow must start with an assessment of compressibility. The flow velocity estimation is much lower than the speed of sound in the liquid metal and by realizing this, compressibility effects can be neglected. (5)

(5) Szekely covers this in greater detail in his text.

The transmission of acoustic information, how fast pressure fluctuations translate through the fluid correlates inversely to the average size of the turbulent eddies. The speed of sound through water is $\sim 1485 \text{ms}^{-1}$ while in liquid platinum it is $\sim 2400 \text{ms}^{-1}$. (6) The speed of sound when multiplied by density results in the characteristic impedance of the medium. Water's characteristic impedance is $\sim 1.5 \times 10^6 \text{N*s*m}^{-3}$ while platinum's acoustic impedance is $\sim 51.26 \times 10^6 \text{N*s*m}^{-3}$. Higher acoustic impedance reduces the mean turbulent eddy size, and this should be considered when analyzing simulation results based on a fluid similar to water. Since the impedance is higher for platinum, the attenuation of small eddies should be greater than simulation results predict.

The suppression of turbulence in metal flows is also aided by the high surface tension of the liquid. Liquid metals have surface tensions much larger than water based fluids. The surface tension of water is $\sim 0.07 \text{Nm}^{-1}$ while the value for platinum is closer to $\sim 1.8 \text{Nm}^{-1}$ (7).

The dynamic viscosity of liquid platinum is $\sim 7.1 \times 10^{-3} \text{Pa s}$ at its melting point (7), while water at ambient temperature has a viscosity of $\sim 1 \times 10^{-3} \text{Pa s}$. This difference is roughly equivalent to the difference between milk and water. Thus, it is expected that there will be less splashing in reality than shown in simulation. As such, for the same arguments above, iterating the mold design based on the results of fluid simulations using

water is acceptable because the results of the simulation will overestimate the severity of splashing, entrainment, and turbulence.

The dimensionless modified Weber number is the ratio of kinetic energy to surface energy. The dimensionless Weber number can be summarized as the product of density (ρ), velocity squared, and characteristic length (L) divided by the surface tension (γ).

$$\begin{aligned} W_e &= \rho v^2 D \gamma^{-1} & 1 \\ W_{e_{\text{modified}}} &= W_e / 48 & 2 \\ W_{e_{\text{modified}}} &= E_{\text{kinetic}} / E_{\text{surface}} & 3 \end{aligned}$$

When the Weber number exceeds unity there is a strong chance for gas entrainment. Observing the ratio of density to surface tension as $\sim 10,000$ we can see that the Weber number during platinum casting will be greater than unity in channels of $\sim 1\text{mm}$ when the velocity is greater than $\sim 0.25\text{ms}^{-1}$.

Campbell suggests a constant fluid-gas interface speed of near 1ms^{-1} to reduce entrainment of gas. The estimated metal entry speed into the mold is $\sim 10\text{ms}^{-1}$ which correlates to a Weber number of almost 100. This reveals that the fluid will splash and break up, entraining air or other mold gas. Alternatively, when the fluid separates the surface will begin to solidify and this can lead to cold shuts, as seen in Figure 1A. A Weber number this high confirms casting under vacuum is a sound practice, though this may not completely resolve cold shuts.

The flow into the mold has a high Reynolds number indicating that the inertial forces are much greater than the viscous damping forces. Normally this would lead a high probability for a transition from laminar to turbulent flow. Analyzing the centrifugal casting process the Reynolds number was calculated to be near 36,000. This is based on the viscosity reported by (7) and a hydraulic diameter of 1mm. In channel flow, as in a water pipe, the transition from laminar flow to turbulent normally occurs between $Re \sim 2,200$ and $Re \sim 4,000$ as indicated on the Moody Diagram. Though, as discussed by (8), it is possible to suppress the transition from laminar to turbulent flow up to Reynolds number of $\sim 40,000$.

The suppression of the laminar to turbulent transition at a higher Reynolds number is complex; there are three flow path modifications that can be made. As reported by Gad-el-Hak riblets may be added running in the direction of the flow. Small riblets allow pressure fluctuation rarefaction upstream of the flow by creating a quiescent and compliant boundary layer. Without these riblets pressure fluctuations are reflected by the walls and grow. The riblets act to dissipate this growth and reduce turbulence when placed parallel to the direction of flow.

Riblets also increase the heat transfer by increasing the ratio of perimeter to area per unit length of the flow path. Increasing the super heat can offset this increase in circumference to area ratio, but requires calculation and thermochemical inspection prior to implementation to determine if there will be any detrimental reactions with the mold or atmosphere. Chvorinov's rule; which relates solidification time (t) to the effective

enthalpy of fusion (H_f') and volume to surface area ratio of the section (V/A), both squared, by a constant (C) that collects thermodynamic property constants, can be used to compare different section geometries.

$$t = C(H_f')^2 \left(\frac{V}{A}\right)^2 \quad 4$$

The Effective enthalpy of fusion (H_f') combines the standard enthalpy of fusion (H_f) with the heat capacity of the metal (C_p) multiplied by the difference between the casting temperature (T) and the melting temperature (T_m). The difference between casting temperature and melting temperature is the superheat.

$$H_f' = H_f + C_p(T - T_m) \quad 5$$

The additional super heat needed to maintain the same solidification time can be calculated from equations 4&5. Figure 3 illustrates the additional superheat needed to maintain the same solidification time for three different geometries all of unit area. To compare these geometries, the circular cross section is calculated with no superheat.

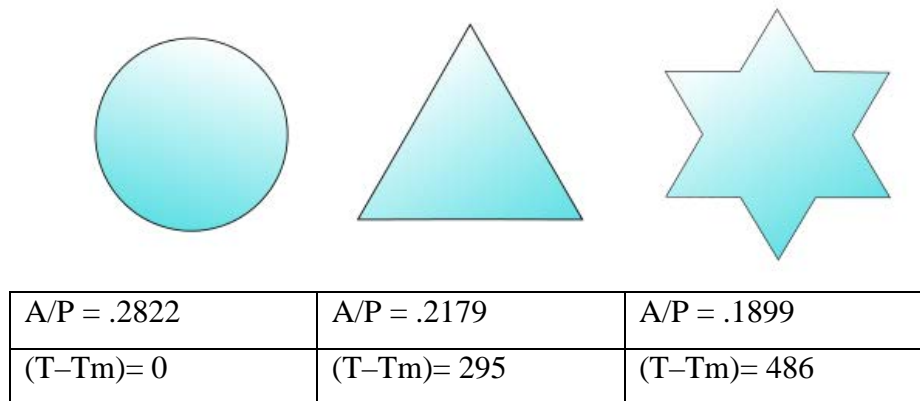


Figure 3: As can be seen from above, per unit length into the page, a decrease in the area to perimeter ratio requires an increase in super heat to maintain the same solidification time. The ratio of enthalpy of fusion to specific heat is estimated at 1000:1 based on data taken from Smithells and is relatively constant for metals.

The idea of riblets is correlated to the second method of reducing turbulence, reducing the effective hydraulic diameter by introducing interior corners. The effective hydraulic diameter can be estimated by the largest circle that can be inscribed in the flow cross section. As the aspect ratio, or faceting of the cross sections changes a reduction in turbulence with a nearly constant flow rate can be observed as reported by Svoboda and reproduced in Figure 4.



Figure 4: Both cross sections have the same area, but turbulence was notably reduced with the cruciform flow geometry.

The third geometric modification that can be made to manage turbulence is to lower local pressure before the metal enters the cavity by increasing the flow cross section. A divergent area will reduce the local pressure and will encourage turbulent eddies to dissipate. This is also discussed qualitatively by Grad-el-Hak, Campbell, and Szekely.

The “Casting Handbook” and the ASM Handbook on casting both cover rigging design in detail. Further inspiration for flow paths can be found by consulting fitting style loss tables found in volumes such as Mark’s Engineering Handbook. By inspecting head loss for different geometries a casting engineer can estimate how a mold will fill qualitatively, which most times is adequate provided the other casting variables are also controlled.

Fundamentally this line of reasoning should lead the casting engineer to conclude that the metal needs to pass through a screen like set of narrow passages to dissipate turbulence. This is standard practice for many aluminum foundries. Though, as shown by the analysis of cross section shape to additional super heat required, this is not an option for metals that solidify quickly such as platinum. Hence it is up to the casting engineer to find a balance between turbulence dissipation, (entrainment reduction), and solidification time. As evidenced by Figure 1A displacement of mold gas in the cavity and the minimization of splashing are the most relevant aspects of fluid flow to consider for platinum casting.

2.2 Filling vs Feeding

Returning to the discussion of fluidity it should be noted that increasing fluidity not only allows the metal to flow a longer distance in a channel, increasing the probability the mold will fill completely, but also helps with feeding during solidification. As discussed by Campbell alloys that have a long freezing range; are more dendritic than

eutectic, exhibit approximately four times lower fluidity than eutectic alloys. As such, alloy development to balance casting and physical properties should always be in the forefront of foundry management.(9)

As the metal is solidifying, from thin sections to thick, it is shrinking. This shrinkage is, for the most part, a cause of internal void formation. Normally the morphology of these voids is jagged because of internal tensile failure. If the alloy has narrow freezing range, substantially free of dendritic solidification, these pores can have a spherical shape because the metal remains fluid even after failing in tension. Voids are normally formed where the metal has been last to cool. This most commonly leads to porosity found in the center of the casting. Because platinum alloys have a high casting temperature, and part geometries have a high surface area to volume ratio, shrinkage porosity due to a lack of feeding is seen throughout the casting. Dendrite formation significantly reduces the metals' ability to feed shrinkage. Figure 5 below gives an illustrated depiction of feeding.

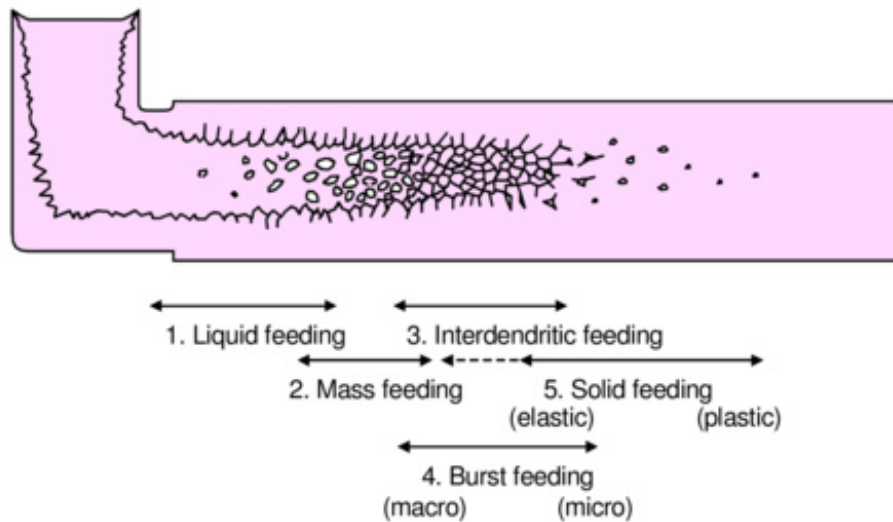


Figure 5: Campbell's illustration of feeding mechanisms. See his work for a more complete discussion on feeding.

Figure 6 shows the solidification structure of the Pt-5%Ru alloy. Dendritic solidification is noted with pores forming at grain boundaries and between dendrite arms.

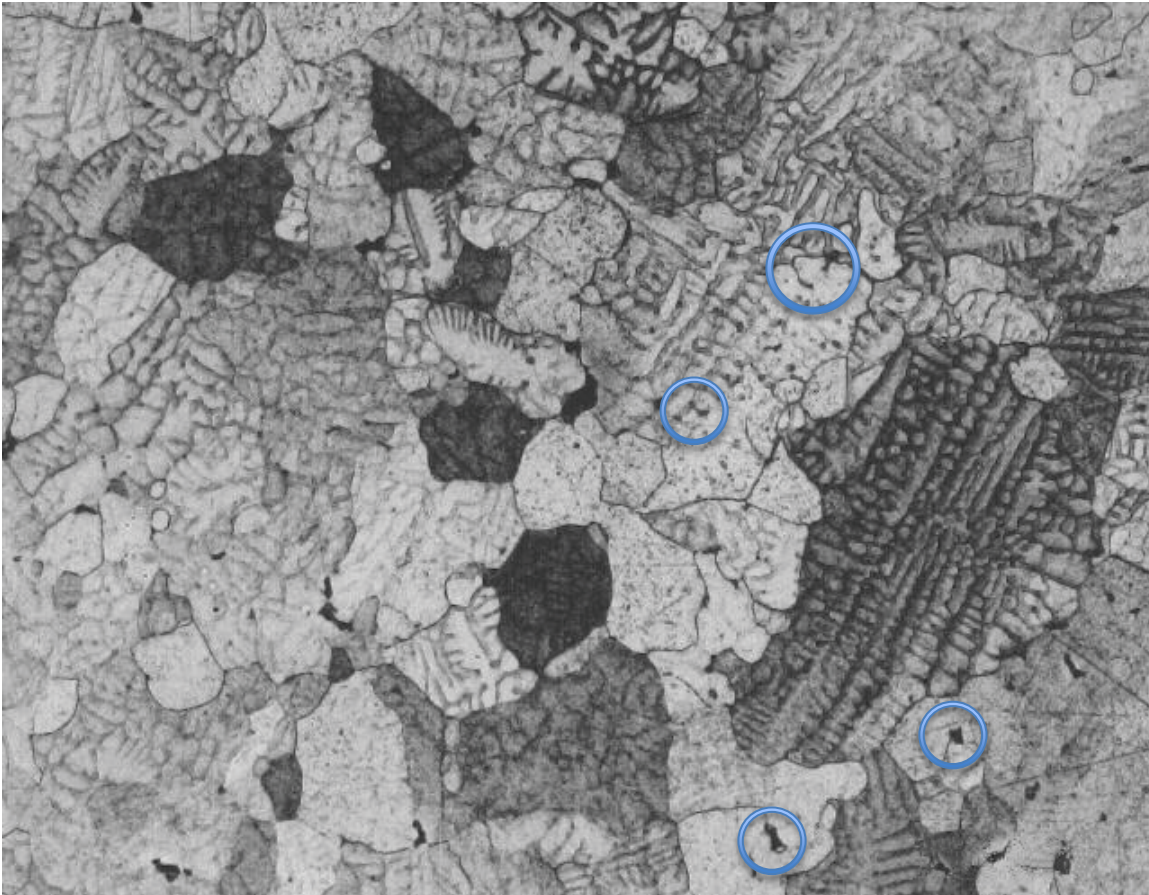


Figure 6: Dendritic solidification structure of the Pt-5%Ru alloy from (10) Circle indicate pores that have formed either at grain boundaries or in between dendrite arms.

The dendrites grow from the walls into the flow creating obstacles. Thermal dendrites, those forming spontaneously from local temperature or pressure fluctuations, along with dendrites broken from the wall significantly inhibit the flow of liquid metal to solidifying sections.

Again, as discussed by Campbell the feeding of long freezing range alloys is approximately a factor of four less than that of a short freezing range alloy. If the alloy is strictly set by extraneous requirements it is up to the casting engineer to find a solution to the feeding problem.

There are two main avenues that can be pursued to this end. One is to increase the superheat. With a higher superheat the metal will take longer to solidify because it will have to reject more energy to the mold. This thermal energy will be stored in the heat capacity of the metal, which will stay liquid longer in the center of the casting allowing more time for feeding to take place.

The second option the casting engineer can exploit is to increase the section thickness of the feeding system. By ensuring the part solidifies from the thin sections to the thick feeding can be encouraged. Installing heavy sections near gates and filling from multiple locations enhance feeding.

2.3 Flow Simulation

As discussed by Grad-el-Hak flow simulation and visualization are valuable tools when designing flow systems. The stochastic nature of multiphase, free surface and high Reynolds number flow makes an exact solution difficult, but approximate solutions often yield enough qualitative and quantitative information to assist design. For the casting engineer simulations can identify low pressure areas that are prone to entrainment, the location of hydraulic jumps, and areas prone to jetting, such that the rigging system can be modified. Removing these trouble spots will allow the mold to fill smoothly and with minimal entrainment. This section covers:

- Lagrangian, Eulerian, or Lattice-Boltzmann simulation algorithms
- Software selection
- Validation
- Limitations

There are three main approaches to computational fluid dynamics problems. These are the Eulerian, Lagrangian, and Lattice-Boltzmann methods. The Eulerian method tracks flow field properties at specific locations using a fixed grid to discretize the geometry. The Lagrangian method shifts with the movement of the fluid tracking each particle and its flow properties. Both of these methods involve solving the Navier-Stokes equations through an iterative process. Sometimes they are combined, as when tracking the progression of a free surface, for efficiency. The Lagrangian approach is effective at tracking the fluid while the Eulerian is more efficient to track the air, a part of the system that is generally less complex owing to the density and viscosity differences. There are usually free surface tracking algorithms that attempt to capture the physics of surface tension, and bubbles. In general these approaches become computationally expensive as layers are added to improve resolution.

The Lattice-Boltzmann method (LBM) discretizes the fluid into particles that are both streaming and colliding. This algorithm is more efficient because it defines a simple interaction equation between volume elements then progress from time step to time step. By solving the velocity and pressure flow field from particle-particle reactions the many body problem of the two previous methods is averted.

One of the best free surface tools available for analyzing casting geometry has been developed by the film industry to animate ocean dynamics. The film industry requires efficient algorithms that produce results that capture the various length scales exhibited by turbulent eddy formation and growth. As a design tool the casting industry requires simulations that are qualitatively real, are computationally efficient, and are easy to implement.

Dr. Nils Thuerey has incorporated a very compact LBM solver into the open source animation program Blender (11). Blender can import a computer generated mold and, by adding some fluid control volumes, fill that mold with fluid. A brief user guide for developing a fluid simulation is attached as appendix A. Figure 7 shows some flow simulation results from initial work produced with Blender.

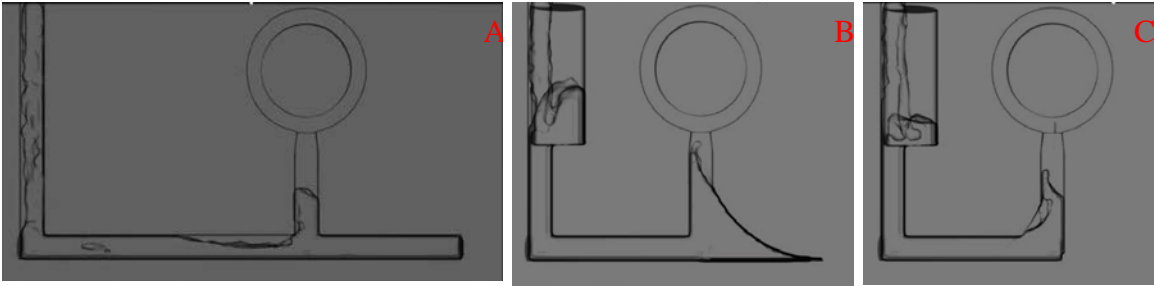


Figure 7: Some preliminary visualizations to look at splashing and jetting in the rigging. Entrainment can be seen in the pouring cups of the center and right images.

The American Institute of Aeronautics and Astronautics defines validation as:
The process of determining the degree to which a model is an accurate representation of the real world from the perspective of the intended uses of the model. (AIAA G-077-1998)

This has been interpreted as, “Solving the right equations”. Mold filling simulations have been performed as a qualitative way to assess bubble entrainment, splashing, and turbulence. To validate this, a quantitative comparison of a drop falling on a bath is shown in Figure 8 below.



Figure 8: The image on the left has been generated by Blender while the image on the right was captured with a high speed camera.¹

From Figure 8 the similarity in fluid structure after the splash is evident. Without the need for further analysis this shows that Blender adequately represents reality.

¹ Left, Blender: <http://www.youtube.com/watch?v=2owqK5Ky64E>

Right, High speed: <http://www.youtube.com/watch?v=5KIOadlOxKc>

3. Heat Flow

3.1 General Considerations of Heat Flow

There are two distinct temperatures to discuss in casting; the temperature above the melting point the metal is poured (the superheat), and the temperature of the mold. The superheat governs aspects of the fluid properties, while the combination of superheat and mold temperature governs the heat flow during solidification. Other aspects involved in considering the heat flow from the metal during solidification are the material properties of the mold and the section geometry. These will be discussed in subsequent sections.

Temperature is one of the easiest variables to control in the casting operation. It simply requires more energy input prior to pouring the metal into the mold. In a lumped thermal model, as is appropriate in casting operations to estimate the transient heat transfer time and thus time to solidification, temperature proportionally increases solidification time.

The empirical validation of heat transfer out during casting was pioneered by Chvorinov in 1960. Perhaps most recently a brief investigation into the filling and solidification of metallurgical grade tin in pyrex tubes was performed (12). From this investigation the length the metal flowed, the fluidity (for a full discussion on concept of fluidity see Campbell), increased with increasing superheat. This is to be intuitively expected, because even though the heat transfer rate also increases with superheat, there is still more energy stored in the heat capacity of the metal that needs to be dissipated. Fluidity also encompasses the metal flow conditions, but this will be discussed in a subsequent section.

From a simple heat transfer analysis the solidification time can be estimated based on half the effective diameter. The most complete derivation of the equation below comes from Poirier but also available from Flemings and Campbell. It is based on the results obtained from Chvorinov.

$$\frac{V}{A} = \frac{2}{\sqrt{\pi}} \left\{ \frac{T_m - T_i}{\rho_i H_f} \right\} \sqrt{\rho k C_p} \sqrt{t} \quad 6$$

V	Volume (cm ³)	H_f	Enthalpy of Fusion (W g ⁻¹)
A	Area (cm ²)	k	Mold thermal conductivity
T_m	Metal Melting Point (K)	ρ	Mold Density
T_i	Mold Temperature (K)	C_p	Mold Heat Capacity
ρ_i	Metal Density	t	Time in seconds

The above equation assumes a semi-infinite mold. This model also assumes that there is no heat transfer resistance at the mold metal interface and that the temperature in the solidified metal is constant. This model is validated by Chvorinov's data.

To account for super heat, the enthalpy of fusion (H_f) can be combined with the additional energy stored in the heat capacity of the liquid metal in a term designated the effective enthalpy of fusion (H_f').

$$H_f' = H_f + C_p(T - T_m) \quad 7$$

Where T is the casting temperature and T_m is the melting temperature of the metal. Inserting effective enthalpy of fusion into the heat flow analysis above, the solidification time as a function of superheat and mold material can be investigated. As shown in Figure 9.

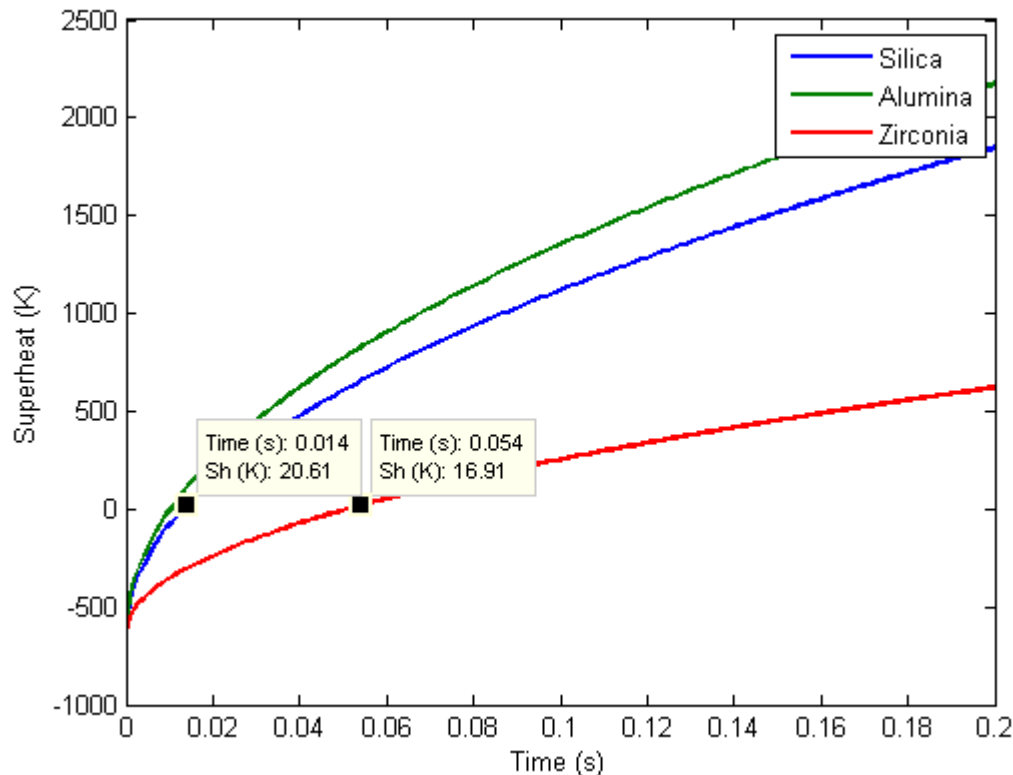


Figure 9: For three different ceramics, silica, alumina, and zirconia superheat is plotted against solidification time. The geometry used to produce this plot was a circular pipe with a one millimeter radius. Table 1 below lists thermodynamic values for the ceramic materials.

Zirconia's high density and specific heat suggest that, from Chvorinov's explicit relation, much less superheat can be used to significantly increase solidification time when compared to silica or alumina.

The conclusion to be drawn from this thermal analysis is that superheat increases solidification time. As such the practical limit of superheat is reached as a result of chemical reactions with the atmosphere or mold material. If the mold material erodes, decomposes, or reacts with the metal a reduction in superheat is required. Until this point, more superheat will lead to better castings by enhancing flow into fine detail and promoting feeding.

Though this conclusion is not surprising it wasn't immediately clear that solidification time was so strongly correlated with the physical properties of the mold material. From the literature the most relevant mold parameter is the melting point. Here it is shown that melting point, while important is only one aspect of choosing the correct mold ceramic.

4. Mold Ceramic

4.1 General Considerations for Mold Ceramics

As discussed by Kingery and Carniglia(13) the criteria used to evaluate the applicability of a refractory system are; toxicity; thermochemical stability; melting point; and mechanical durability.

When choosing an oxide as a mold material, availability and cost must also be considered. These will be dealt with explicitly in a subsequent section; the author has discounted ceramics with a price per pound that is greater than one hundred times the current silica based refractory. The reader is referenced to the economic modeling section for a more thorough discussion of this choice.

This section will cover:

- Toxicity
- Thermochemical Stability & Melting Point
- Mechanical Durability
- Making a slurry
- Binding the ceramic

4.2 Toxicity

From all possible oxides available naturally, (excluding carbides, nitrides, and borides which have associated problems such as volatile thermal decomposition and oxidation), there are several that need to be discounted due to their toxicity. Beryllia, thoria, chromia, and urania are toxic enough that their benefit to the foundry is negligible. The cost of additional safety precautions needed when handling these materials outweighs their benefit. This results in an even shorter list of available ceramics that can be used as molding materials.

4.3 Thermochemical Stability & Melting Point

Both Mellor(14)and Vines(15) cite that when melted in magnesia or calcia crucibles platinum becomes hard to work. This could be a result of the alloy absorbing the gas phase oxide, or providing a surface for catalytic reduction and the formation of a platinum alkali intermetallic. Both magnesia and calcia have high vapor pressures at the melting point of platinum. As a result these refractories are unsuitable mold materials for platinum casting in spite of their low cost.

Silica will also form a volatile sub oxide at the casting temperature of platinum (14). This has been observed by Ainsley et. al. when heavy sections of platinum have been cast in silica molds. Based on these observations it is clear that a primarily silica

based mold material is substandard. Davis et. al.(15-17) report on the decomposition of mullite above 1600C and note the evolution of silicon monoxide in atmospheres with low oxygen partial pressure. Similar results are expected from zirconium silicate (zircon).

Magnesium aluminate spinel is another promising oxide system in which platinum has almost negligible solubility.(18) They suggest that this is because platinum coordinates to a IV fold planer oxide instead of a tetrahedral structure, and that this planer coordination elastically strains the octahedral or tetrahedral sites in the oxide enough to substantially reduce solubility. There was no other explanation found in the literature for why platinum had such a low solubility in Mg-Al spinel.

Though spinel has a melting point over 2000C it also suffers from lattice inversion at high temperatures. Aluminum will swap from an octahedral coordination to a tetrahedral coordination near 800C. This causes a volume change that can lead to cracking. Spinel can be stabilized with the addition of alumina or by optimizing process parameters.

From the above discussion; oxides that possess melting points above 1800C, are reasonably available, and will not adversely react with platinum are few. Table 1 lists these oxides and relevant data.

Ceramic	Melting Point [°C]	Thermal Conductivity [W (cm K) ⁻¹] (approx. values at 2000C or M.P.)	% Linear expansion at 1000C	Heat Capacity @1000C [J (g K) ⁻¹]	Density [g cm ⁻³]	Bulk Cost [\$ m ⁻³]
SiO ₂	1723	.15	.04 (vitrified)	1.161	2.65	\$1869.52
Al ₂ O ₃	2054	.112	.82	1.227	3.95	\$11669.07
MgAl ₂ O ₄ (Spinel)	2135	.085	.6	1.238	3.95 (est)	\$15065.29
ZrO ₂ - Calcium stabilized	2715	.0328	.99	0.635	5.68	\$85151.34
Y ₂ O ₃	2410	.030	~1	0.562	5.01	\$47604.63
TiO ₂	1857	-	-	-	4.23	\$45228.93

Table 1: Compiled physical properties of oxides that can be used as mold materials for platinum casting.²

Because titania provides no mechanical, chemical, or economic benefit over alumina it will not be discussed. Spinel is included in the above table because it was considered to be the refractory of choice before some of its physical properties came to light.

² All data except for yttria comes from Carniglia. Data for yttria has been extrapolated from Kline et. al. and Goldstein et. al. Cost data; for silica was supplied by Lane Ind.; for alumina and spinel, Brenntag Specialties; for zirconia, Remet Corp.; and for titania and yttria, Stanford Materials.

4.4 Mechanical Durability

Mold material strength is calculated as the modulus of rupture (MOR). The material is formed into bars that are subsequently broken in a three point bending machine. The maximum load, normalized by the cross sectional area is the modulus of rupture, with units of stress. For homogeneous materials the modulus of rupture will equal the tensile stress. For ceramics, and very brittle materials, this is complicated by the inherent presence of defects. Generally the Wiebull modulus is used as the specific failure stress of ceramic materials. The research conducted here did not pursue this because defects are a natural part of the manufacturing process and calculations based on MOR are more relevant when comparing different mold compositions. Because porosity and thus strength can be modified easily by adjusting process variables, such as firing rate and temperature, thermodynamic stability is initially more relevant.

The discussion of mold strength is complicated by the solidification shrinkage of the metal. If the mold material is too strong the metal will not be able to deform the mold and lead to a tensile failure of the metal (a hot tear). If the mold material is too weak the flow of liquid metal will wash away fine detail during casting.

Adding to the strength issue is the issue of vitrification, or glass formation. If the mold material becomes glassy in an interior geometry at the end of solidification it will be in a compressive stress state. This compressive stress will be on the order of the yield stress of the metal, ~200MPa. Amorphous materials that have been cooled in compression are extremely hard. A remarkable example of this property is the Prince Rupert drop. To fracture or abrade the glass the inherent yield stress of the glass plus the compressive loading, in this case the yield stress of the metal, must be overcome. With this understanding it is advisable to find a material that will not form an amorphous phase, and adjust the strength of that material to ensure that it is less than the ultimate tensile strength of the metal. Silica will vitrify while alumina and zirconia are much less likely to. The currently used silica mold material has a green strength (MOR) of 0.92MPa and a fired strength of 2.03MPa. This has proven to work well in most applications. Higher green strength can help reduce mold damage during handling prior to final firing and should be pursued when possible.

Carniglia presents that the best assessment of ceramics resistance to thermal shock is the linear coefficient of thermal expansion. From the above table, alumina has the lowest thermal expansion, though in this regard there is little difference from one ceramic to the next in this list.

Because it is economical to fire the mold ceramic at temperatures less than 1000C and the casting temperature of the metal is over 2000C the mold will suffer a temperature gradient of 1000C at the mold metal interface. This can cause spalling, flaking of the ceramic off the mold walls, at the metal-mold interface.

4.5 Making A Slurry

For flask casting operations the ceramic slurry must be cast around the wax pattern to form a monolithic refractory. The ceramic slurry must have a low enough viscosity to fill fine details, dry without shrinking and cracking, possess enough green strength to support itself, and fire, without cracking, into a dense body. These

requirements are largely controlled by the initial ceramic slurry composition, but are also influenced by heating rates and times.

The two most important aspects of slurry design are particle size distribution and dispersion. As discussed by Norton(19) and Carnigila(13) having a wide particle size distribution increases packing density and lowers slurry rheology. Lower rheology is also accomplished by manipulating the surface potential of the particles by altering the pH.

A high solid volume fraction reduces the likelihood of cracks forming during drying and shrinkage during firing. When the solid particles take up more than 75% of the volume of the slurry cracking during drying is completely avoided. At these loadings, when a slow heating ramp is used during firing, particle growth is encouraged, the matrix coarsens and shrinkage is again minimized. With a high solid volume fraction and wide particle size distribution after drying Van der Waals forces provide sufficient green strength.

With high solids loading rheology is reduced by a ball bearing effect. The increased density also reduces rheology by lowering the dilatancy, volume expansion induced by flow. It should also be noted that the surface roughness of the cast part is approximate to the average particle size radius.

By adjusting the slurry pH to maximize the positive zeta potential on the particles the lowest apparent viscosity will be observed. The pH that corresponds to the maximum positive zeta potential is oxide specific. Table 2 lists possible ceramic oxides with the pH that corresponds to the maximum positive zeta potential. Effective dispersion is usually accomplished at low pH, but can also be done at high pH. Carnigila notes that dispersions at low pH exhibit a lower apparent viscosity than those dispersed at high pH. (19)

Ceramic System	Maximum Zeta Potential (pH)	Point of Zero Charge (pH)
Silica	<0	1.5
Alumina	5	9.2
Zirconia	4	7

Table 2: The pH of maximum positive zeta potential is dependent on the metal oxide acid-base character.(13)

4.6 Binding the Ceramic

The current silica based refractories use magnesium phosphate as a binder to provide both the low temperature and high temperature strength. This binder is reacted from magnesium oxide and phosphoric acid just prior to the refractory being cast into the flask. Though it has shown reasonable strength, and is as thermally stable as the silica itself, as previously discussed magnesium oxide will evolve a vapor species at the casting temperatures of platinum. Phosphorous oxides also form low melting point eutectics with platinum in addition to decomposing upon reaching temperatures of ~1600C. (16, 20)

Ceramics can also be bound together with colloid suspensions. Colloidal silica is the binder of choice for many shell casting operations. There are also colloids of alumina,

zirconia, and yttria among others. These colloids are pH stabilized and can be mixed directly with the bulk ceramic to make a dense mold. When fired these colloids exhibit a lower melting temperature than their bulk counterparts. This reduction is normally around 5% of the melting point. The lower melting colloid helps control sintering rate and provides more design flexibility.

5. Cost Model

5.1 Profit, Yield, Price and Cost

Cost is a fundamental tenant of any manufacturing process. The cost model of a foundry hinges on successful castings that can be delivered as products. By minimizing the cost per part in labor and materials and maximizing the yield, a foundry will maximize its profits. What follows is a simple cost-benefit analysis to compare the additional material costs with the yield from a better refractory. The foundry cost model is illustrated in the equation below

$$\text{Profit/Casting} = \text{Yield} * (\text{Price} - \text{Cost}) - (1-\text{Yield}) * \text{Cost} \quad 8$$

Here cost includes the metal, ceramic, and the associated labor to; make the mold, cast, and prepare the casting for secondary machining. Price represents the sale price of the part. For this analysis price is taken to be constant.

What is not obvious from the above equation is the relationship between yield and cost. Working under the assumption that there is some minimum cost to produce a part, and that there are diminishing returns for increasing yield by increasing the cost, the equation below can be written. The assumption that there are diminishing returns to yield from by increasing cost is appropriate based on the idea that theoretically increasing monetary investment in the casting process to reduce variation will eventually lead to a near 100% yield, and there is relatively high yield after very little initial investment. Because there are many costs associated with the processes that have been lumped, it is unclear what the exponent represents in real terms. The next section will derive the additional yield required to justify the increase in material cost encountered when changing mold ceramic.

$$\text{Yield} = 1 - \{ \text{Cost} \}^{-X} \quad 9$$

The operational costs are fixed and can be neglected for this analysis, being lumped into the “cost” variable. By substituting the yield equation into the profit equation we can see that there will be an optimum that is most sensitive to our cost per casting. Here we can see that there will be negative profit if our price is lower than our cost over yield.

$$\text{Profit/casting} = \text{Price} * \{ 1 - \text{Cost}^{-X} \} - \text{Cost} \quad 10$$

Or

$$\text{Profit/casting} = \text{Price} * \text{Yield} - \text{Cost} \quad 11$$

When the profit equation above is differentiated with respect to cost and set to zero to find local maxima the relationship between price and cost where profit will be maximal can be found.

$$\text{@ max Profit: Price} = \text{Cost}^{(1+X)} * X^{-1} \quad 12$$

To verify this model the exponential variable “X” needs to be determined by fitting the curve to data. As such, differing ceramic systems can be fit with this model and very little auxiliary data to determine which ceramic system will maximize profits by increasing yield for their associated cost. By lumping the variables and inspecting the rates of change of profit against those variables it is assumed that there is little or no correlation between variables. This is to say that costs associated with using higher quality ceramic are not associated with increased secondary processing costs.

5.2 Justifying A Higher Cost Ceramic

Table 3 lists the most promising ceramic systems and their cost per cubic inch. Volume is used to normalize the cost due to bulk density differences.

Ceramic System	Bulk Cost [$\$ \text{m}^{-3}$]
Silica	\$1869.52
Alumina	\$11669.07
Zirconia	\$85151.34

Table 3: Some systems and their associated cost per volume.

To determine if an increase in material cost will increase profits the relationship between yield and cost must be determined. To simplify the math it is assumed that with the current SiO₂ system there are no profits. This allows the representation of price in terms of cost and yield.

$$\text{@ Profit} = 0 \quad \text{Price} = \text{Cost}/\text{Yield} \quad 13$$

To compare one ceramic to another the profit equations for both are equated. Below the subscript Si indicates silica.

$$\text{Profit} > \text{Profit}_{\text{Si}} \quad 14$$

$$\text{Price} * \text{Yield} - \text{Cost} > \text{Price} * \text{Yield}_{\text{Si}} - \text{Cost}_{\text{Si}} \quad 15$$

$$\text{Yield} > (\text{Cost} - \text{Cost}_{\text{Si}}) / \text{Price} + \text{Yield}_{\text{Si}} \quad 16$$

Equation (13) can be substituted into (16) yielding

$$\text{Yield} > \{ (\text{Cost} - \text{Cost}_{\text{Si}}) / \text{Cost}_{\text{Si}} + 1 \} \text{Yield}_{\text{Si}} \quad 17$$

From the above equation we can now calculate the minimum additional yield necessary to justify shifting to a higher cost ceramic. The missing part of this analysis is the measured yield when silica is used as the ceramic. For this work yield from silica refractory is estimated to be 75%.

Using the bulk cost estimation from Table 3, the above analysis shows that the increase in cost associated with switching to an alumina based ceramic from a silica based one is not economical even if yield approaches 100%.

This economic analysis is by no means complete, but does provide a framework to build a complete model on. Secondary processing costs have not been considered, nor has the necessity of moving to a better performing ceramic been weighted.

A key component of assessing yield is part geometry. Parts with filigree will need to be cast with enormous superheat, and the standard silica based material will not work driving up the value of a more suitable ceramic.

This analysis simply compares the incremental improvement needed across the board to justify switching to a higher cost ceramic. This analysis also neglects any additional processing costs, such as acid etching the ceramic off the metal, though these should differ only slightly from one ceramic to the next.

The model most notably neglects secondary processing costs and rework. The goal here was to determine if yield alone could justify switching to a higher cost mold material. A more thorough analysis needs to be undertaken to truly compare ceramics.

6. Methods

6.1 Overview of Methods

The investigation into the platinum casting process was initiated by benchmarking the established variables. For an industry standard refractory the modulus of rupture was determined using a three point bending test, the superheat and mold temperatures were noted, and the flow geometry was modeled.

Initial tests were conducted with an increased superheat. This lead, as supported by Ainsley, to mold breakdown. It quickly became evident that a better mold material was needed to support higher superheats. Simultaneously the fluid flow path was being simulated and tested. (16)

6.2 Ceramic Testing Scheme

An iterative methodology was used to test new ceramic systems. This process is illustrated in Figure 10. The cycle was started with an initial literature review and has been run for each ceramic composition tested.

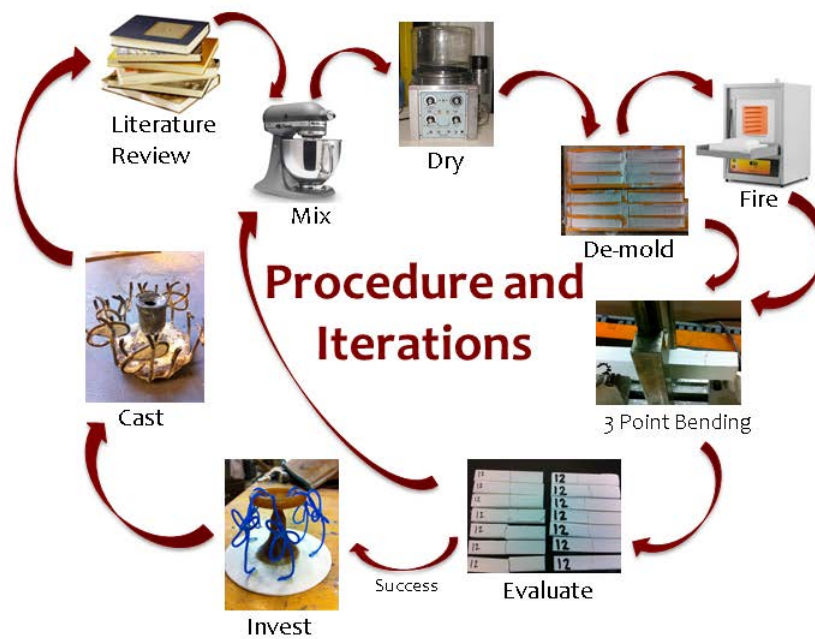


Figure 10: Illustration of the testing and iteration process used to evaluate changes in the casting process.

7. Results and Observations

7.1 Molds

7.1.1 Ceramic Recipes

A full list of all refractory compositions tried and notes on different additives is compiled as Appendix B. The most promising mold recipes are listed here for silica, alumina, and zirconia.

The silica mold material that was developed is based on the commercially available Lane system. (Available from Lane Industries). It consists of a trimodal distribution of silica particles suspended with a 70/30 mixture of 85% phosphoric and 37% hydrochloric acid. Equal weights of each powder with mean particle diameters of ~2, ~4, and ~19 microns were combined to broaden the distribution.

Binding was accomplished by the addition of magnesium oxide. It was found that MgO with a lower specific surface area, and thus less reactive, provided more working time to prepare the molds. The supplied MgO from Land Ind. appeared to be light burned, or simply calcined, meaning that it was very reactive, while dead burned, or hard burned MgO from Premier Ind. worked better.

The slurry is mixed by adding the acid to water, then the silica powders to the acid solution all while mixing. When the powder is fully dispersed, ~10min of mixing, the MgO is added. Mixing is continued for two minutes. The slurry is then evacuated and poured into the flasks. Table 4 lists the recipe. Table 5 displays the original silica recipe that was provided by the manufacturer.

250g	2 μ m silica
250g	19 μ m silica
100g	4 μ m silica
11ml	70/30 85% H ₃ PO ₄ / 37% HCl
127ml	Deionized Water
6.6g	Dead Burned MgO

Table 4: The most promising silica based mold system. Water and acid are combined and while mixing silica powder is added. Mixing was difficult at first. Premixing silica powder is recommended but not needed. After 10min of mixing the MgO is added. Mixing is continued for 2 min then the slurry is evacuated to remove bubbles. After evacuation the slurry is placed into the flask.

613g	2 μ m silica
12.7	4 μ m silica
12.2ml	70/30 85% H ₃ PO ₄ / 37% HCl
162.3ml	Deionized Water
2g	Activated MgO

Table 5: The original silica recipe as supplied from the manufacturer (Lane Industries)

The alumina system that was developed mimicked the silica system. It was noticed that alumina by itself started to react with the acid because the viscosity of the slurry increased with long mixing times. Thus shorter mixing times were used and mixing was done at a higher rate. Ingredients were added in the same manner as the silica mold material. Again dead burned MgO was used as the binder.

The particle size distribution was significantly different for the alumina system. Here two particle sizes were used, a fine distribution of 0 to 0.2mm, and a coarse distribution of 0.2-0.6mm. The recipe for the alumina system is displayed in Table 6.

60g	0.2-0.6mm Alumina
100g	0-0.2mm Alumina
11ml	70/30 85% H ₃ PO ₄ / 37% HCl
127ml	Deionized Water
6.6g	Dead Burned MgO

Table 6: Recipe for alumina based mold material. Water and acid are combined and while mixing alumina powder is added. Mixing was difficult at first. Premixing alumina powder is recommended but not needed. After 10min of mixing the MgO is added. Mixing is continued for 2 min then the slurry is evacuated to remove bubbles. After evacuation the slurry is poured into the flask.

The zirconia system was substantially different from the silica and alumina systems. It makes use of a colloidal suspension of nano particles of zirconia stabilized in suspension by acetic acid to a pH of 3.5³. This formula was less free flowing than the silica or alumina ones, but with slight vibration leveled easily.

³ The zirconia sol is produced by Nyacol Nano Technologies, Inc. and is sold directly by them or through the Remet Corporation.

100g	0-.044mm Zirconia
100g	0.15-0.30mm Zirconia
18ml	20wt% 5-10nm Zirconia Sol

Table 7: Recipe for zirconia based mold material. The powders can be pre mixed, but this isn't necessary.

7.1.2 Firing Schedules

After investment, molds were left undisturbed on the bench for 4hrs. Then they were placed in an environmental chamber at 80C and 10%RH for 12hrs. Dewaxing followed at 150C for 3hrs.

A firing schedule was constructed based on the recommended schedule for the commercial silica based mold material. The initial ramp was 1C/min to 400C from room temperature. The molds were held at 400C for 4hrs to allow the silica mold to slowly transition into the cristobalite phase. Though other mold materials were not subject to this phase transition the firing schedule remained constant. After holding at 400C for 4hrs the ramp of 1C/min was continued up to 1000C. Molds were held at 1000C for a minimum of 2hr and up to 6hr before being cast. No variation in mold quality was observed by holding for longer times.

7.1.3 Mold Material Tests

Modulus of rupture data for plausible compositions can be found in Appendix B. This section reports the MOR of the standard silica, improved silica, alumina, and zirconia mold materials that were developed.

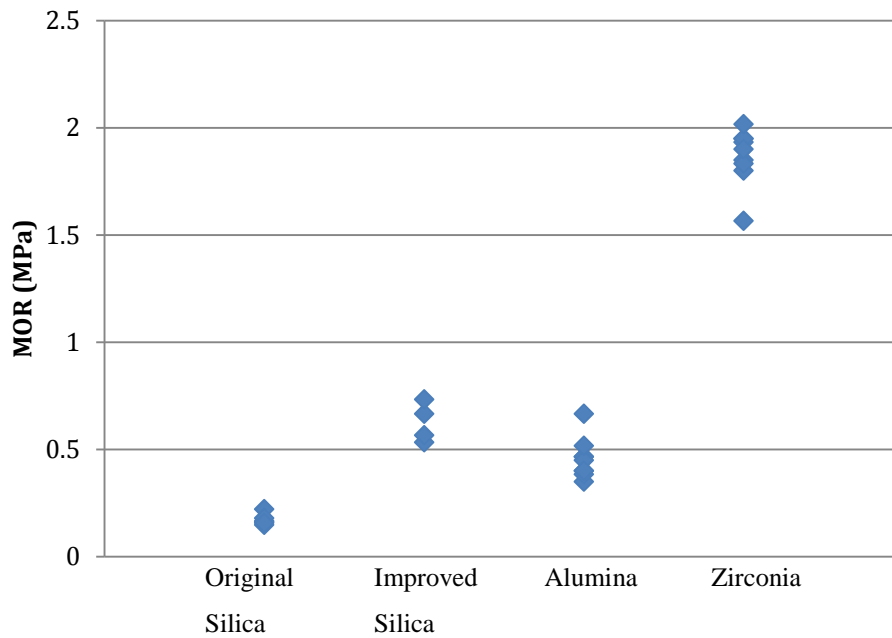


Figure 11: MOR of the unfired most promising ceramics.

Figure 11 reveals the impact of particle size distribution on ceramic strength. It also shows that the zirconia system is approaching the empirically accepted ideal value of 2MPa.

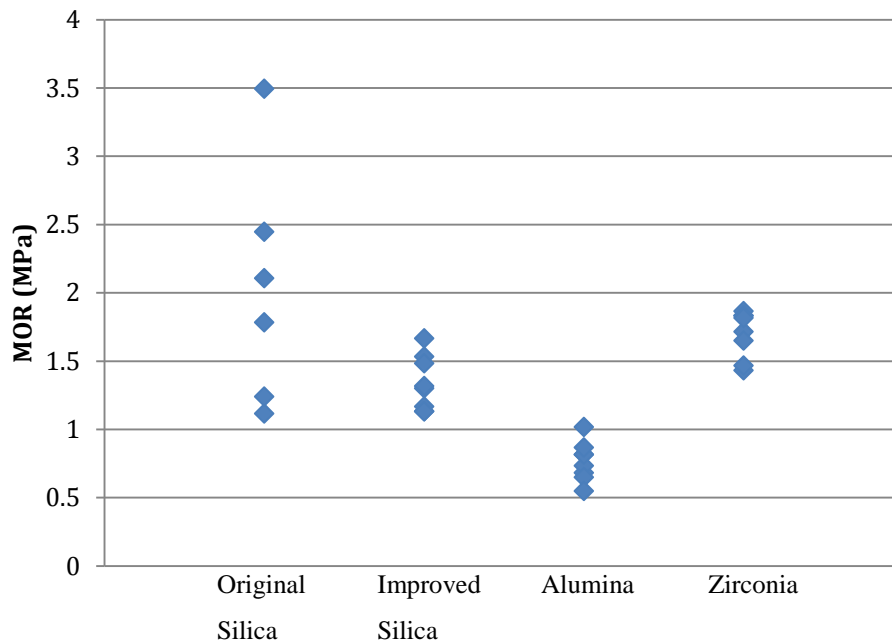


Figure 12: MOR of the fired most promising ceramics.

Figure 12 has notable scatter in the original silica recipe. This could be a result of using the more reactive magnesia. Even though the original recipe appears more

appealing than the improved silica recipe, the improved recipe suffers much less shrinkage upon drying and thus is less prone to cracking.

7.1.4 Other Mold Considerations

Though zirconia has a higher strength than silica or alumina it was prone to cracking while drying. This was likely due to the sol precursor forming a vapor barrier on the free surface of the mold. These molds need an addition of something like starch or oil that will a percolating network for vapor to escape. The silica and alumina molds have an internal reaction, the formation of magnesium and/or aluminum phosphate that displaces the water as it leaves the slurry.

7.2 Fluid Simulation Results

Fluid simulations used an initial flow rate of 10ms^{-1} and a gravity value of 150ms^{-2} which had been estimated from the casting machine's operating parameters. This section will cover:

- Simulation workflow
- Simulations of single ring filling
- Runner and gate design
- Effect of a screen
- Effect of a conical diffuser
- Benchmark
- Evolution of sprue design

7.2.1 Simulation Workflow

The workflow for simulating fluids starts with the creation of a 3D representation of the casting geometry. This geometry is then digitally assembled into an assembly. The assembled tree is then exported from the design software (Solidworks) and imported into Blender. The reader is referenced to Solidworks extensive tutorial library for generating positives and assembling them into trees. The reader is also referenced to Appendix A for detailed information on importing the geometry and performing the simulation in Blender.

Once the rendering finished, splashing and entrainment were qualitatively observed. The rigging was then modified and re-tested. This process is graphically represented in Figure 13.

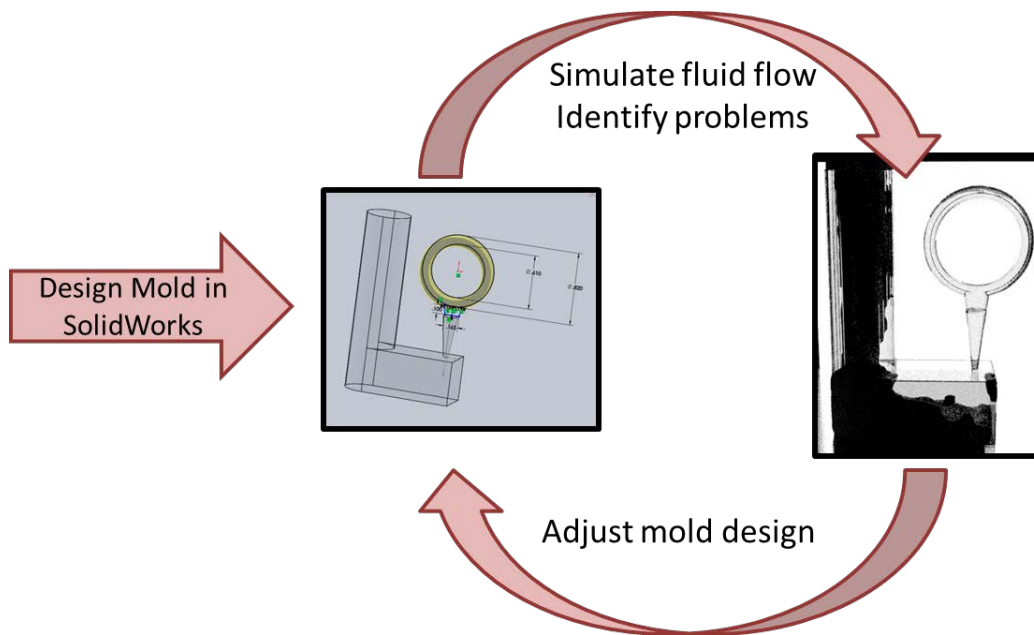


Figure 13: The fluid simulation design process

7.2.2 Single Ring Filling

The simulation iteration cycle started with an investigation of how one ring filled with different runner and gate geometries. These results were briefly displayed in Figure 7 and are reprinted in Figure 14.

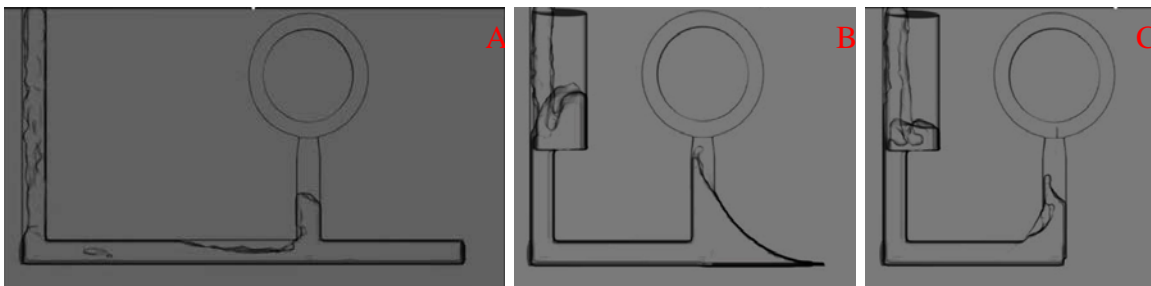


Figure 14: A representative selection of some initial designs.

Figure 14A is representative of splashing found by varying the angle between the gate and runner and changing the distance between the sprue and the gate. A similar amount of splashing was observed in all iterations of these parameters.

Figure 14B summarizes an investigation into dissipation of the hydraulic jump associated with the flow hitting a sharp corner before filling the part. The reflection of the flow causes splashing that is of similar magnitude to that observed in Figure 14A. Various sweeps and truncated sweeps were tested. Splashing was observed in all geometries to some degree.

Figure 14C followed from Figure 14B. A local low pressure region can be seen on the left side of gate. This low pressure region is unacceptable because it promotes entrainment and this geometry was not developed further. The reader is referenced to Appendix C for a full list of tests.

Figure 14B and C both also investigated reducing the fluid velocity entering the part cavity by increasing the overall cross section of the flow path at the height that the part started. This was accomplished by increasing the sprue diameter at the height of the ring. Though the velocity was lower during filling the observed entrainment in the sprue did not encourage further investigation of this idea.

7.2.3 Effect of a Screen

Screens comprised of very thin plates running parallel to the flow path caused a dramatic reduction in turbulence. This coincides with Svoboda's results from reducing hydraulic diameter. This was concluded to be the best theoretical option though it was rejected because it is impractical to fabricate. . Figure 15 is a captured frame from a ring that has a screen in its gate.

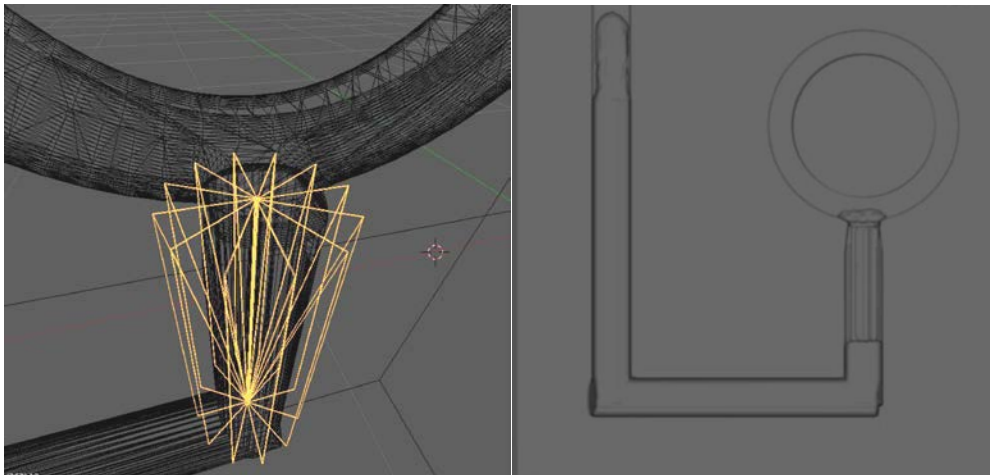


Figure 15: The image on the left shows how the screen is oriented while the image on the right shows the smooth filling of the cavity.

7.2.4 Effect of a Conical Diffuser

Flow rate can be retarded if cross sectional area is increased. Increasing the cross sectional area also allows turbulent eddies to grow and dissipate. These facts inspired the use of a flared gate attaching the sprue to part. This design worked significantly better than straight gates as shown in Figure 16.

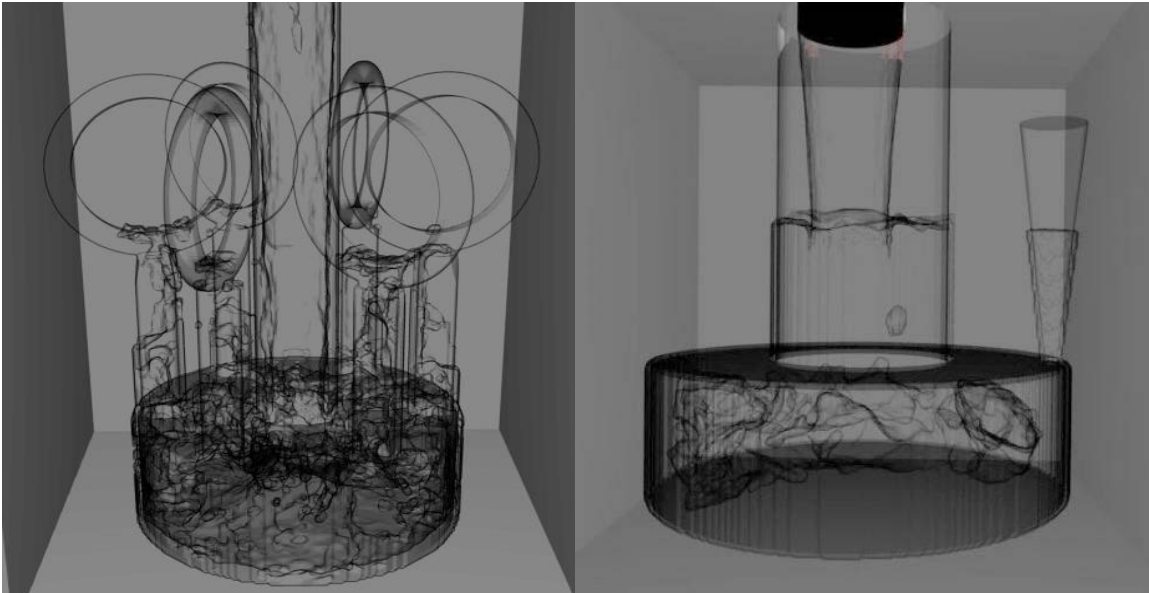


Figure 16: The image on the left shows turbulence entering into the part cavity while the figure on the right shows a smooth fluid front progressing up the gate.

Along with the exploration of diffusing the flow the use of a plenum was also explored. The large volume helped dissipate turbulence and reduced the flow velocity so the parts filled with a smooth fluid front.

7.2.5 Final Design and Benchmark

By combining the above a design that incorporates conical diffusers and fills from the bottom was developed. This design was benchmarked against the traditional “button” design. The results of this comparison are showing in Figure 17. Each frame in Figure 17 represents an elapsed time of approximately 0.042 seconds. The simulations estimate that the mold fills completely in ~0.4 seconds, which is in good agreement with an estimation based on casting machine parameters.

The last frames in Figure 17 show the proposed design free of turbulence and the parts beginning to fill smoothly. This is compared to the “button” design at the same time which continues to show turbulence.

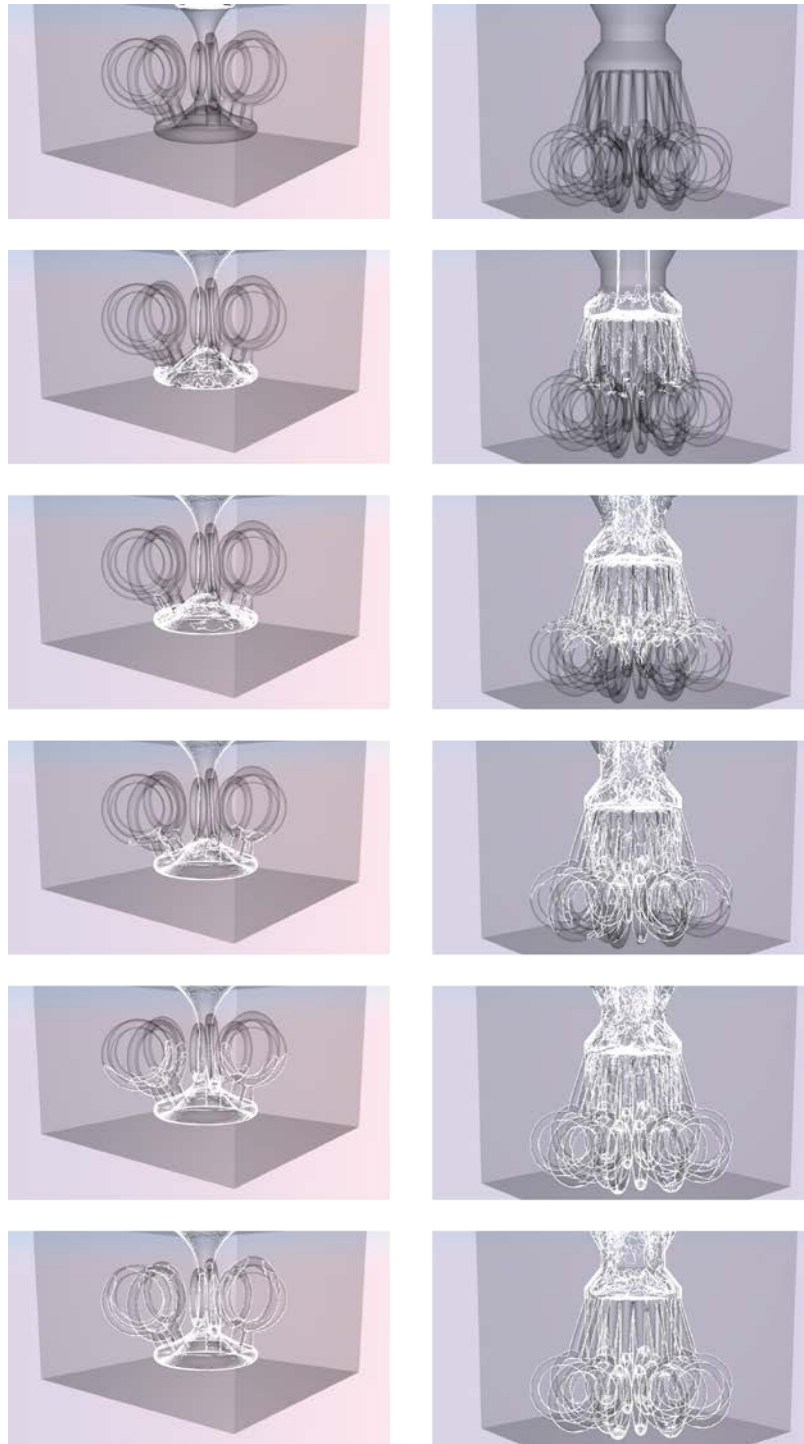


Figure 17: A side by side comparison of eight frames of the redesigned sprue (left) and the “button” design (right). Frames are shown at the same time so turbulence can be compared. The total elapsed time from top to bottom is ~0.29 seconds.

7.3 Casting Results

To assess both filling and heat flow a pretzel shaped geometry was cast out of an iron-niobium-chrome alloy in the three different mold materials developed. The solidification structure of this alloy can be seen in Figure 18. The metal was cast at the same temperature for each mold material (2000C).

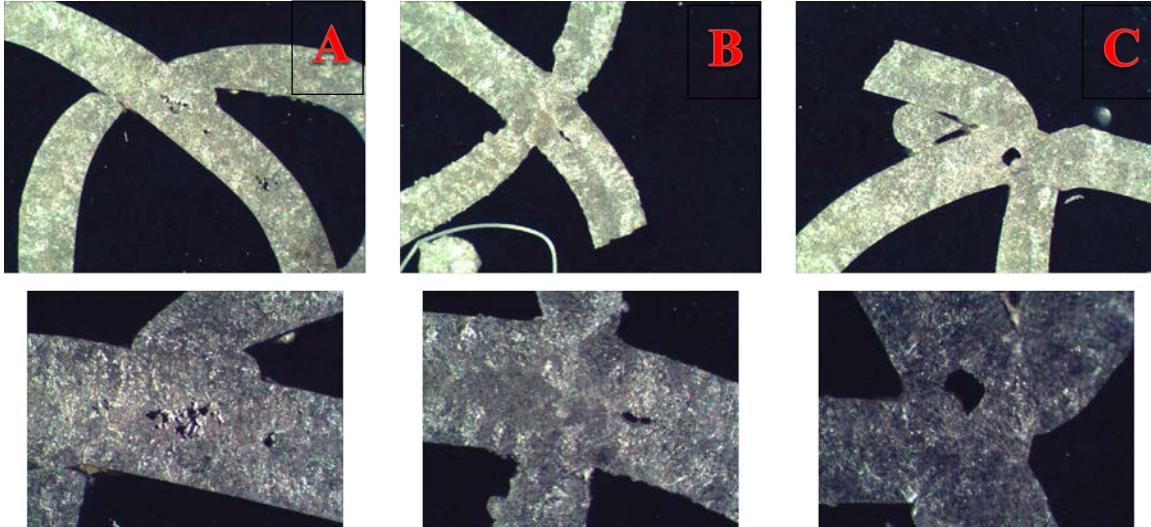


Figure 18: Casting results; (A) shows a pore that formed in the improved geometry silica mold, (B) shows a pore that formed in the alumina mold, (C) shows a pore that formed in the zirconia mold. The second line reflects the same pores at high magnification.

The different pore morphologies displayed in Figure 18 support the conclusion that minimizing $C_p\rho\kappa$ for the mold material increases solidification time and promotes feeding which decreases interdendritic porosity. The pores in the silica and alumina mold materials (Figure 18 A&B) show the same jagged structure as those observed in the Pt-5Ru alloys. The pore in the zirconia based mold material has much smoother edges. This suggests that the pore was due to an entrained bubble and was not formed as a result of solidification. It should also be noted that the edges of the casting that used an alumina based mold are much rougher than those of the silica or zirconia molds. This suggests that there was some metal mold interaction, the mold material thermally decomposed, or was simply not strong enough.

8. Conclusions from Results and Future Work

8.1 Fluid Flow

The results gained from this investigation clearly show that bottom filling parts after having the liquid metal flow through a diffusing area reduces turbulence. This reduction in turbulence will reduce entrained bubbles being captured in the final product. Though the casting results are inconclusive in terms of entrained gas, the methodology developed here should be widely applicable to the casting industry in general.

8.2 Heat Flow

Casting results support the hypothesis derived from Chvorinov's relation that delaying solidification by decreasing the heat diffusivity, $C_p\rho\kappa$, for the mold will increase feeding and reduce porosity.

8.3 Mold Ceramic and Economics

Developing other ceramic options must be tempered by economic considerations. For future casting operations the improved silica ceramic should be used. It is more tolerant to process variation and has the same cost as the original recipe.

Magnesium phosphate bonded alumina should not be pursued as a viable alternative to silica. The low strength outweighs the higher thermal resistance. Other bonding mechanisms could be explored that may increase the strength of the system. Xue and Chen have published some promising results sintering alumina at 1000C with colloidal titania and both copper and boron salts to create a fugitive liquid phase. This work could be expanded to develop a new mold material.(21)

From the casting results, alumina is no better for solidification than silica. Zircon, another possibility, costs ~\$2/lb and thus could provide a compromise between insulating capability and economy. Yttria is also a possibility, but has very similar properties and cost compared to zirconia. Yttria is commercially supplied by Stanford Materials and Nyacol in the same product forms as the zirconia used to develop the mold recipe in this work.

The zirconia system needs further development to become a useful flask casting slurry. Cracking on drying was a significant problem even with the high green and fired strength. Fumed silica is an additive that could provide porosity and prevent cracking. Hydrolyzed cellulose could also provide enough porosity for the water to escape through. Simply diluting the sol with alcohol could also help reduce cracking on drying but will also most likely reduce strength.

For implementation, an initial dip coat of the wax in a zirconia slurry would be the best compromise, creating a thermally insulating layer around the mold cavity and minimizing the cost of the mold material.

9. References

References

1. Matysiak, H.; Michalski, J.; Balkowiec, A.; Sikorski, K.; Kurzydowski, K. J. Surface defects of investment castings of turbopfan engine components made of IN713C nickel superalloy. **2009**, 27.
2. Jehn, H. High temperature behaviour of platinum group metals in oxidizing atmospheres. *Journal of the Less Common Metals* **1984**, 100, 321-339.
3. Ferguson, P.; Westmacott, K. H.; Fisher, R. M.; Dahmen, U. COUPLED DIFFUSION OF CARBON-ATOMS AND VACANCIES IN PLATINUM. **1985**, 1, 53-60.
4. Miller, D.; Keraan, T.; Park-Ross, P.; Husemeyer, V.; Brey, A.; Khan, I.; Lang, C. Casting platinum jewellery alloys. *Platinum Metals Review* **2005**, 49, 174-182.
5. Szekely, J. *Fluid flow phenomena in metals processing*; Academic Press: New York, 1979; , pp 437.
6. Ishikawa, T.; Paradis, P. F.; Koike, N. Non-contact thermophysical property measurements of liquid and supercooled platinum. *Japanese Journal of Applied Physics Part 1-Regular Papers Brief Communications & Review Papers* **2006**, 45.
7. Ishikawa, T.; Paradis, P. F.; Okada, J. T.; Watanabe, Y. Viscosity measurements of molten refractory metals using an electrostatic levitator. *Measurement Science and Technology* **2012**, 23, 25305-25313.
8. Gad-el-Hak, M. *Flow control: passive, active, and reactive flow management*; Cambridge University Press: 2007; .
9. Campbell, J. Complete casting handbook [electronic resource] : metal casting processes, metallurgy, techniques and design. 1.

10. Frye, T.; Fischer-Buehner, J. The Quest for Quality: Optimising Platinum Casting for 21st Century Needs. *Platinum Metals Review* **2012**, *56*, 155-161.
11. Thürey, N. *Physically Based Animation of Free Surface Flows with the Lattice Boltzmann Method: Physikalische Animation Von Strömungen Mit Freien Oberflächen Mit Der Lattice-Boltzmann-Methode*; Verlag Dr. Hut: 2007; .
12. Pai, B.; Jones, H. Effect of experimental variables on casting fluidity and fluid life of liquid tin. *Materials science and technology* **1985**, *1*, 398-404.
13. Carnigila, S. C.; Barna, G. L. *Handbook of Industrial Refractories Technology*. **1991**.
14. Mellor, J. W. *A comprehensive treatise on inorganic and theoretical chemistry. Supplement*; Longmans, Green: London, New York, 1956-; .
15. Vines, R. F.; International Nickel Company *The platinum metals and their alloys*; The International nickel Co: New York, N.Y., 1941; , pp 2.
16. Ainsley, G.; Bourne, A.; Rushforth, R. Platinum Investment Casting Alloys. *Platinum Metals Review* **1978**, *22*, 78-87.
17. Davis, R. F.; AKSAY, I. A.; PASK, J. A. Decomposition of mullite. *J Am Ceram Soc* **2006**, *55*, 98-101.
18. Brenan, J. M.; Finnigan, C. F.; McDonough, W. F.; Homolova, V. Experimental constraints on the partitioning of Ru, Rh, Ir, Pt and Pd between chromite and silicate melt: The importance of ferric iron. **2012**, *302*, 16-32.
19. Norton, F. H. *Refractories*. **1949**.
20. Ullmann, F. *Ullmann's encyclopedia of industrial chemistry* [electronic resource]. *6*.
21. Xue, L. A.; Chen, I. W. Low-Temperature Sintering of Alumina with Liquid-Forming Additives. *J Am Ceram Soc* **1991**, *74*, 2011-2013.

10. Appendix A – Using Blender

Importing the Mold

1. Make the positive of the mold in SolidWorks. You will usually need to make an assembly to attach different parts. Try to keep the assembly to as few parts as possible. It doesn't matter how complicated each part is.
 - a. Don't save an assembly as a part. SolidWorks won't be able to save the .STL file.
2. Save the assembly as a .STL file. The assembly will become multiple separate .STL files, one file for each part. Keep the files in the same directory.
3. Open up Blender and click File – Import. Hold down SHIFT and click each filename to select all the .STL files in your assembly. This will import each part as a separate mesh, but all the meshes will be properly aligned in space.
4. Press “A” to deselect everything. Right-click any one part of your assembly. It should be the only thing highlighted. Now, press “B” for border select, and left click and drag to draw a box around your entire mold assembly. Make sure only the mold itself is selected and not the camera or light source. (Hitting “5” on the number pad to go into orthographic view mode helps with this). Press “Ctrl+J” or click “Join” on the left hand side to join all the separate parts into one object.
5. Make a cube mesh, or use the cube mesh in the default scene. Scale the mesh (right-click to select it, and press S for “scale”) until it is the size of the mold. You can hit “Z” to go into wireframe mode, so you can see both the cube and the mold. You can hit “S X”, “S Y”, or “S Z” to scale along only the X, Y, or Z axis. Try to make the cube as small as possible while still fitting around the mold. Use orthographic view mode by pressing “5” on the number pad. The shortcuts for side, front, and top views are “1”, “3”, and “7” on the number pad.

- a. You can save time in a later step if you duplicate this cube once you've scaled it properly. Hit Shift-D to duplicate the cube and right click to put it in place. One of the cubes will become the fluid sim domain (see step 12).
6. Now move or scale the cube as necessary such that the main sprue sticks out of the cube a little bit. If you don't have a sprue, you can click the mold mesh, hit TAB to go into Edit mode, and extrude a face by selecting it and hitting "E". Then hit TAB to go out of Edit mode.
7. Hit "A" to deselect everything. Make sure you are in Object mode, not Edit mode, and click the box. Select the inner cube. Click on the Modifiers icon on the right side of the screen (looks like a wrench). Click Add Modifier – Boolean. A box should pop up with a drop down menu with the word "Intersect" selected. Click on this and change "Intersect" to "Difference". Under "Object", choose the mold assembly. It should be the only object to choose. If it's not, it's probably the one with the really long and complicated name. If there are a lot of objects with the same name, the mold parts haven't been properly joined into one object.
8. The cube should now look like the mold shape was carved out of it. If everything looks good, hit "Apply". This permanently changes the cube mesh into a cube with the mold cut out of it.
9. The mold positive should still be visible. Right click to select it and hit "M" to move it to another layer to get it out of the way. Click the second layer (or any layer besides the first) when the box pops up. If the box disappears, you can hit any of the numbers on the top row of the keyboard to move it to that numbered layer (so press anything 2-9).

10. Right-click the cube with the mold shape carved out of it. Click on the Physics tab, and click on “Fluid”. Make the mold a volume-initialized fluid obstacle with free slip.

11. Make more meshes to be fluid inflows and outflows as needed.
 - a. I recommend a volume initialized fluid inflow with an initial velocity in the $-z$ direction above the sprue, and a shell-initialized fluid outflow around the inflow with the bottom face deleted. This outflow will delete any excess fluid that climbs to the top of the mold. To delete the bottom face of the outflow mesh, select it by right-clicking, hit TAB to go into Edit mode, hit CTRL+TAB and press “F” to change the selection mode to “Face”. Right click the dot in the center of the bottom face to select it and hit “Delete”, then “F” to delete the face.

12. Make a cube mesh and scale it so that the mold and all inflows and outflows fit inside it. Make the cube a fluid domain.

Baking

1. There are several domain settings you can change. Change “Viewport display” from “preview” to “final”. Changing the “final resolution” directly affects bake time – use low resolution (40-60) if you want results in the next few minutes, and use high resolution (150+) and let it run overnight to make a nice video.
2. Change the “Real World Size” option in the Physics tab when you have the domain selected. It defaults to 0.5 meters – usually I put this around 0.07 based on the dimensions in my SolidWorks model. This defines the longest axis of the Domain cube to be whatever distance you input and scales the model accordingly.
3. Change the “Simulation End Time” option in the Physics tab. It defaults to 4 seconds. If you change Real World Size, usually your mold will fill much faster

- than 4 seconds. For a real world size of 0.07 m and an inflow velocity of -10 m/s, the mold usually fills in less than 0.5 seconds.
4. To change the gravity, click on the Scene tab on the right hand side and scroll down to Gravity. You can input whatever gravity settings you want (in m/s^2) on this tab. I usually used -150 m/s^2 . (Note: You may have to uncheck “scene gravity” from the scene tab (the one with a light a ball and a cylinder) to adjust gravity in the fluid domain).
 5. Ensure “Remove air bubbles” is unchecked in the Fluid Boundary tab.
 6. When everything is ready, right click the domain object, go to the Physics tab, and click “Bake”.
 7. If Blender crashes, you can try a couple of things:
 - a. Lower your resolution. I haven’t had much success over 200.
 - b. Decrease the time step between frames. To do this, either lower the “simulation end time” or increase the number of frames in the simulation (bottom of the screen).
 - c. Open another instance of Blender. I have no idea why this works.
 8. Some other issues:
 - a. If the fluid leaks out the side of the mold, select the mold, go into edit mode, and “recalculate normals”.
 - b. You can also try subdividing the mold into smaller polygons.
 - c. Changing the resolution also sometimes helps

Rendering

Once the file is done baking, you can render the simulation to save a video of the simulation.

1. Position the camera appropriately. Right-click the camera object to select it, and hit “G” to grab it and move it around. I usually hit “7” on the number pad for top view, zoom out, and pull the camera far away from the mold. Also be sure to hit “R” to rotate the camera so that it’s pointed at the mold.
2. To check and make sure the camera is pointed at the mold, press “0” on the number pad. This will show you the camera view. If it’s not quite perfect, you

- can hold “Shift” and press “F” to go into Camera Fly Mode. In Camera Fly Mode, you can move the mouse up, down, left, or right to pan the camera in that direction, or you can hold down the middle mouse button and move the mouse to translate the camera in that direction.
3. Once the camera is set up, the materials for the mold and the liquid need to be adjusted. To change the color and transparency of the mold, right click the mold to select it, and click on the “Materials” tab on the right side of the screen. I have found that scrolling down to “Transparency” and turning up the “Fresnel” and “Blend” sliders makes the edges of the mold visible but everything else is transparent. You can also append the materials from other .blend files and use them. To do this, click File -> Append, and navigate to the .blend file with the material you want. Click “Material” and hold down Shift and click to select all the materials you want to import.
 4. To change the color and transparency of the *fluid*, click the fluid domain, not the fluid inflow. Adjust the material properties of the fluid domain.
 5. To see if you like the materials, you can click “Render Image” in the Render tab on the right side of the screen (or press F12). An image should render. (If you want to save the image, hit F3).
 6. If everything looks good, you can render an animation. Under the “Render” tab, change the “output directory” option to something other than /tmp\ so that you can find the animation. Change the output from “.PNG frames” to “AVI Raw”. Hit “Render Animation” and let it run!

Tip: Pay attention to how many frames are in the simulation and what the simulation end time is. AVI raw will output at 24 frames per second. If you have the default of 250 frames and a 4 second simulation, the video will play in slow motion, since 250 frames at 24 fps is over 10 seconds.

Also, if you want to use another rendering engine, like Cycles, the materials tab will have completely different settings. If you use Cycles, the “Glass” material looks really good, and you can change the index of refraction under the “IOR” option if you want to.

11. Appendix B – Data on ceramic compositions

This appendix contains notes on the compositions investigated. I referenced compositions are stored in the spreadsheet, “Compiled Mold Data” in the “Data on Ceramic Compositions” directory.

This appendix is organized into several sub sections

- Aggregate – The main ceramic component
- Binder – What holds the aggregate together
- Additives – Chemicals tested to improve rheology and/or strength

Aggregate

Silica – currently being used by Tiffany & Co. An exploration of particle size distribution has shown that tailoring the powder blend can reduce shrinkage as well as increase green and fired strength. Formulas (1-34,40,42,44,F2-4,C13) have focused on this material.

MgO - Dead burned(low specific surface area) MgO was investigated as a crucible material. Formulas (35,39,43,49,C5,C8,C10) explored this material. Crucibles made from this material were very strong, though they lacked thermal shock resistance.

Mullite - Mullite was explored as a possible mold material in formulas (3,5,38,49,50,C12,C14). One very promising composition was developed using CAC as a binding system(formula 50). A significant amount of time was spent trying to form mullite during the firing process. Most of these compositions did not work. In situ mullite formation was investigated in formulas (3,4,6-12,15-23,26-28,44)

Alumina - Alumina was explored as a mold material in formulas(41,45-49,F5,F6).

Spinel - A very promising material due to its thermal properties. It has been explored as a component in formulas (C10,C11) and as the base ceramic in formulas(C1-C4,C6,C8-9,F1).

Zirconia - A very high melting temperature oxide that is very inert, and has high thermal shock resistance. It has high green strength minimal shrinkage, and good fired strength. Formulas (C7,C9-12,F7,C14) investigated this material

Binder

Subsections include acidic and basic binders.

Acid Binders

MgO Phosphate - It provides reasonable strength. It was used in formulas (1-12,F1,F3).

Aluminum Phosphate – A bonding system that was proposed by Kingery as a low temperature setting cement that can be fired up to high temperature. In initial tests in formulas (F5,F6) showed weak fired strength. The molds cracking upon casting.

Colloidal Zirconia Acetate Stabilized – Used in formulas (C6,C13,F7,C14) as a binder. When mixed with zirconia flour it provides excellent dispersion while increasing particle loading. Green strength is reasonable and fired strength acceptable.

Basic Binders

CaO - A highly reactive oxide that readily hydrates to form Van der Waals bonds. It was found to be too reactive to be used as an efficient binder. It was tested in formulas (22,29,46)

Calcium Aluminate Cement - A binder system that resulted in very little shrinkage, but low fired strength. It was used in formulas (48-50,C1-5,C7-12,F2-4)

Additives

Fibers and Matrix modifiers

E-glass fibers – formulas (32,34,39,40,42,43,47,48,49) showed an increase in green strength with a lowering of fired strength

Fiber-Frax alumino-silicate – Have not been quantitatively tested but have been used based in formulas (F1-5,C13) based on the improvements seen from using E-glass.

Polystyrene beads – Were tested as a way to reduce the density and increase permeability. This weakened the ceramic unacceptably and was rejected from further development.

Use of Silicones/Phosphates/Alcohols/Other

BASF 1390 Antifoam – When used in formulas (F2-3,C13) with acid binding systems it caused a significant increase in viscosity, most likely due to polymerization.

Aluminum isopropoxide – Used in formulas (C1,C4), compared to similar formulas (C2), those that used al-propoxide seemed to have a lower viscosity

Poly Vinyl Alcohol – Used in formulas (13,14,17,19-22,25,C3,C4) to combat shrinkage. A wider particle size distribution works much better to combat shrinkage than PVA so investigation into this chemical was abandoned.

Aluminum powder – Tested in formulas (6,7) as a way to cause the slurry to expand during setting. The concentration was too difficult to control to use this reliably. Reactivity is highly pH dependent.

Ammonium phosphate – Used in formulas (13-16) to promote AlPO_4 formation. The neutral salt did not provide enough dispersion force in the slurry and this route was abandoned.

TiO_2 - Used in formulas (25,26,29-34,40,42,48,C11,C13,F7,C14) as an aid to form secondary phases during firing.

PMMA (ADDMIX 15) – Used in formulas (C8-C12) to help with cracking on drying as well as shrinkage. It worked reasonably well but lead to additional shrinkage upon firing.

Use of Acid type additives

Citric acid – Tested in formulas (13,14,17,21,23-40,42-46) citric acid was not effective at deflocculating and dispersing the particles.

Hydrochloric acid – Tested in formulas (1-12,21,34,42,F1,F3,F5) this acid was marginally good at deflocculating and dispersing particles, but its effects on strength were inconclusive and possibly deleterious. It is currently included as a component in the Lane binder.

Polycarboxylic acid – (water reducer) A common Portland cement additive, it seemed have little effect in formulas (15,16,C1,C2,C4), and negative effects when the pH became acidic.

Magnesium citrate – Sol precursor used in formulas (27,28,47,C4) this additive seemed to have little effect.

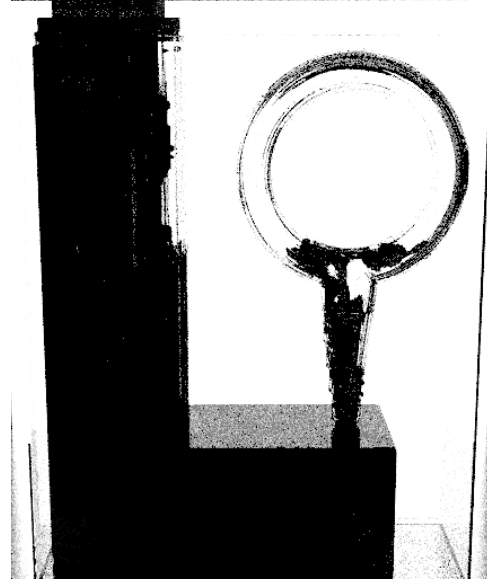
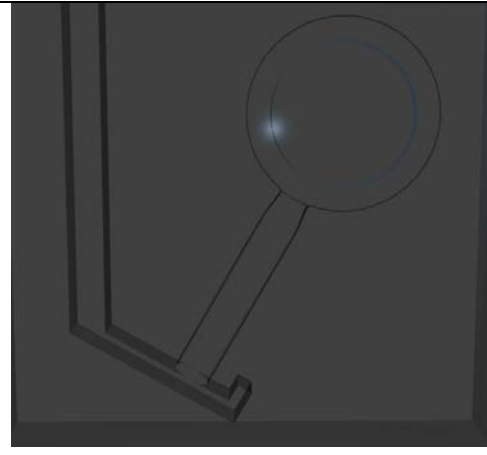
Use of Base type additives

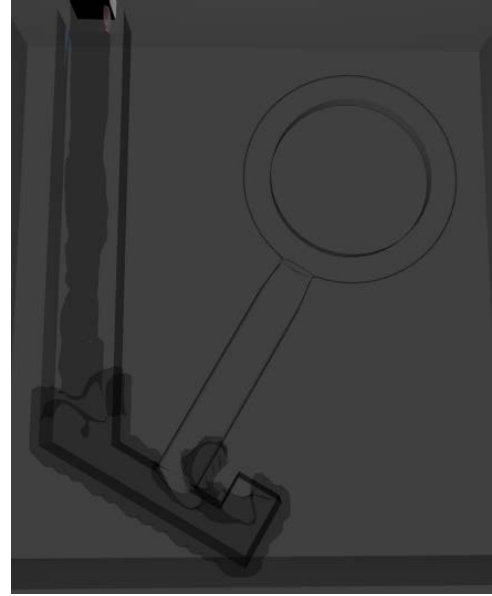
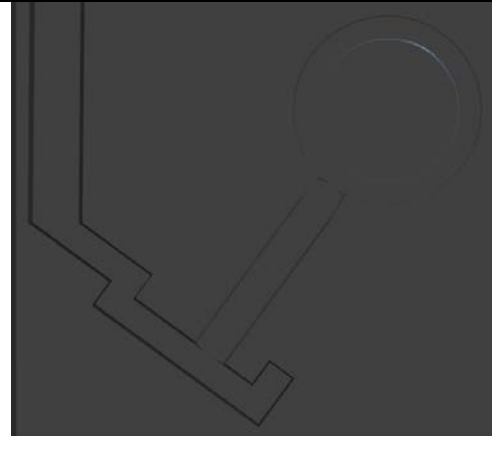
Aluminum hydroxide – Used in formulas (26,29-34,40,42,F5) it was not strong enough to provide reasonable green strength.

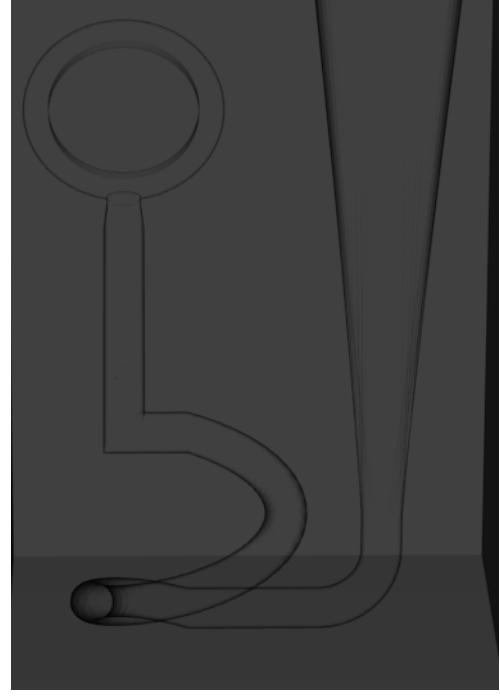
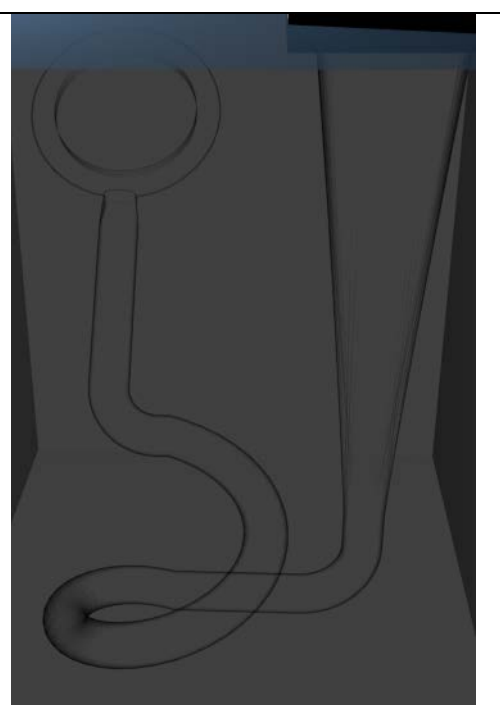
MgO as an additive –Used in formulas (3-5,9-12,24,27,28,42,C10,F1,F3,F7) as an aggregate. Used in formulas (18,19,20,21,25,26,29-35,39-41,43,45-49,C5,C8) as a component of the ceramic system.

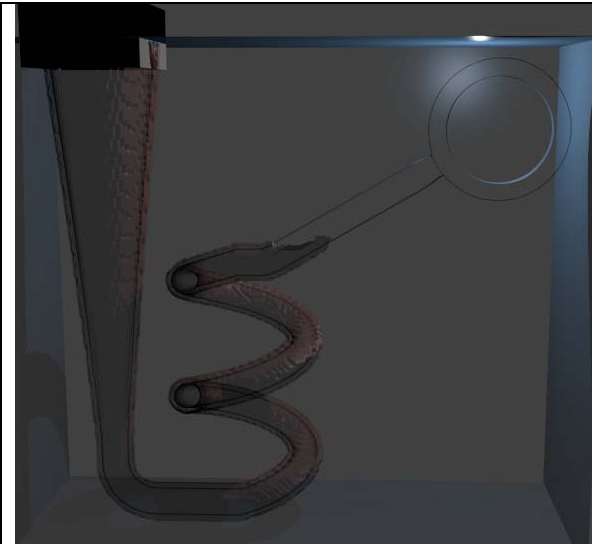
12. Appendix C – Index to Fluid Simulation Results

Related files are located in the “Fluids Simulations” -> “Simulation Files” directory. A picture has been provided for referencing the filename.

 A black and white photograph showing a physical ring sprue assembly. The assembly consists of a circular ring at the top, connected to a vertical stem that ends in a small nozzle. The entire assembly is mounted on a dark, rectangular base. The background is light and slightly textured.	000 - Demo Diffuser
 A 3D CAD model of the ring sprue assembly shown in the photograph above. The model is rendered in a dark gray color with a semi-transparent effect, showing the internal structure of the ring and the stem. The background is a dark, solid color.	001 - Corner Stop After Ring Sprue

 A 3D perspective rendering of a dark grey gate corner. The corner is reinforced with a thickened, rounded section. A circular hole is visible in the upper part of the gate.	<p>002 - Fatter Corner in Gate</p>
 A 3D perspective rendering of a dark grey gate corner, similar to the one above but with a more pronounced, double-thickened corner reinforcement. A circular hole is visible in the upper part of the gate.	<p>003 - Double Corner in Gate</p>

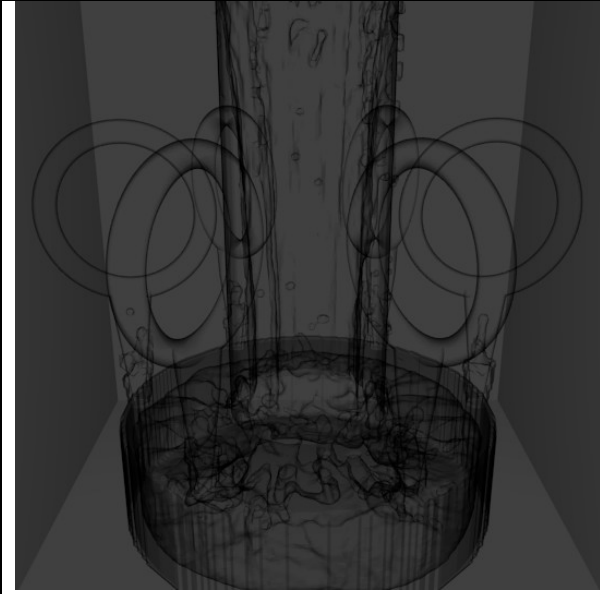
 A 3D rendering of a spiral in a gate. The spiral starts at a circular ring at the top left and winds downwards and to the right, ending at a small sphere at the bottom left. The gate is a dark, rectangular structure with a vertical edge on the right.	<p>004 - One Spiral in Gate</p>
 A 3D rendering of a spiral in a gate, similar to the one above but without a sharp corner. The spiral starts at a circular ring at the top left and winds downwards and to the right, ending at a small sphere at the bottom left. The gate is a dark, rectangular structure with a vertical edge on the right.	<p>005 - One Spiral in Gate, No Corner</p>



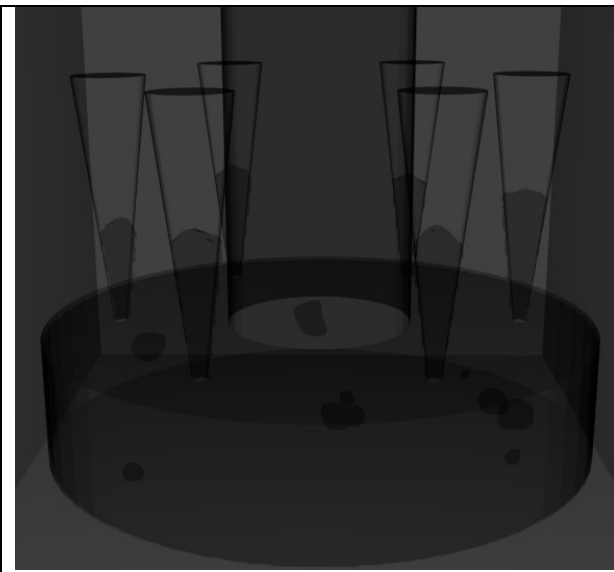
006 - Two Spiral in Gate, No Corner



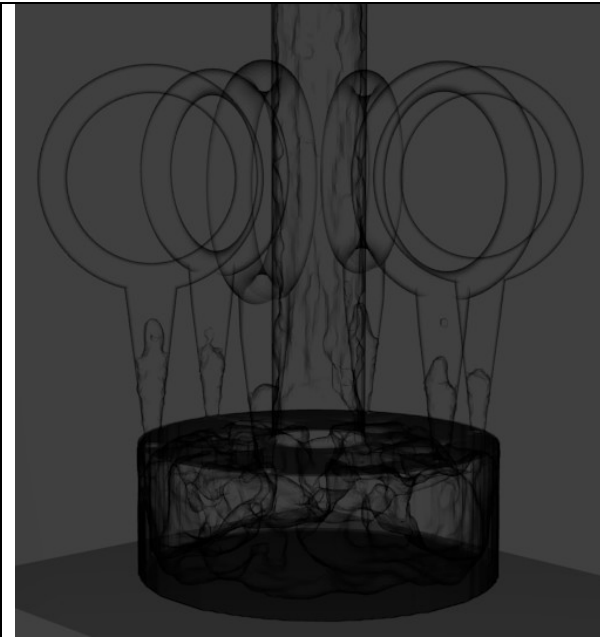
007 - Plenum with One Diffuser



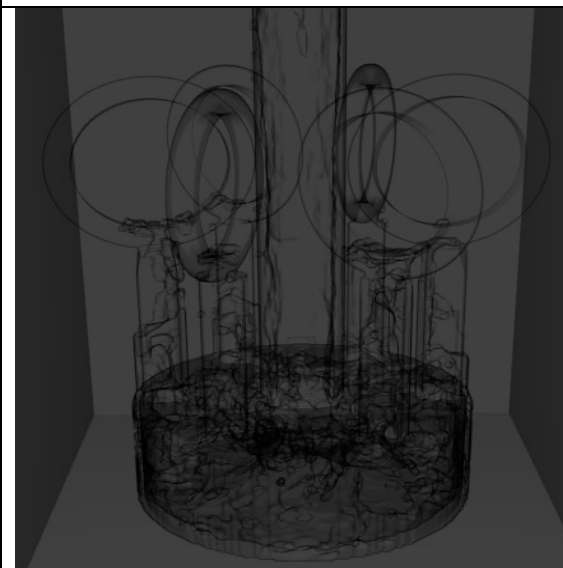
008 - Plenum with Six Diffusers and Rings



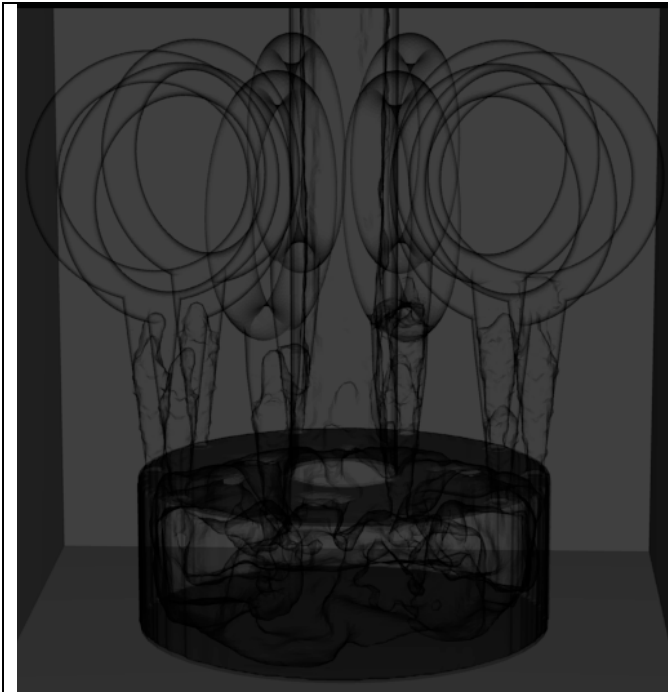
009 - Wider Plenum Six Diffusers



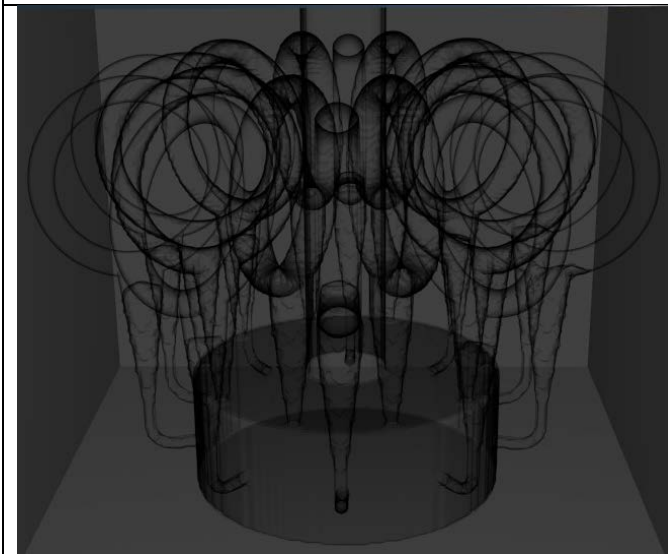
010 - Plenum with Six Diffusers and Rings and Skinnier Sprue



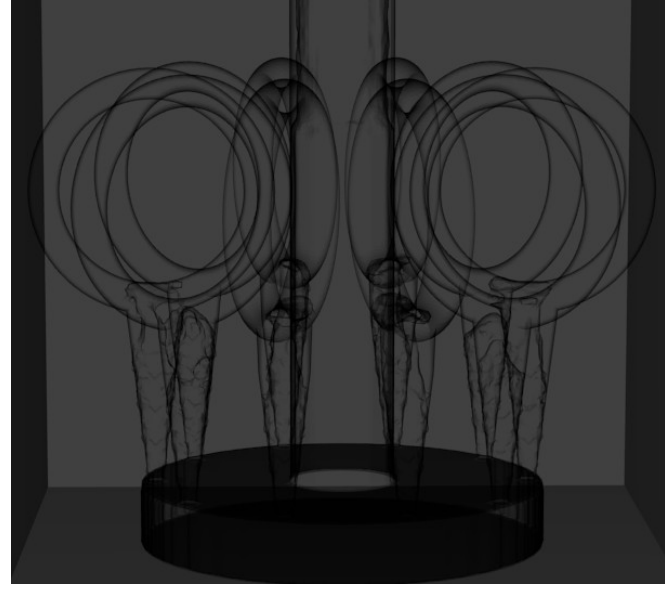
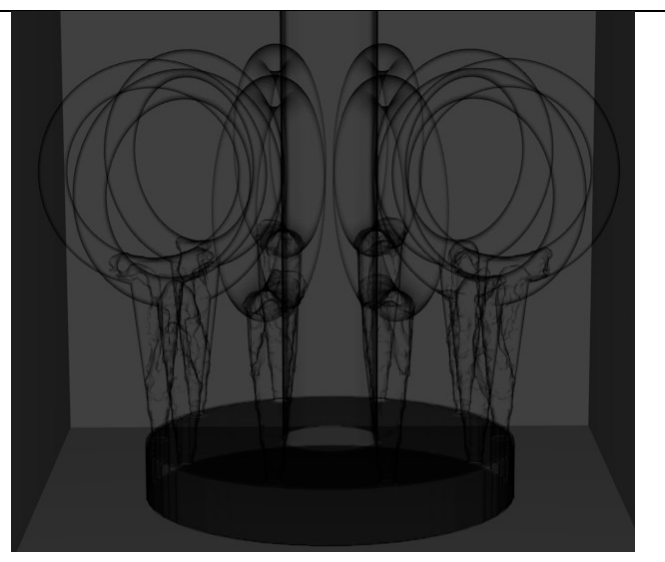
011 - Plenum With Six Rings, No Diffusers

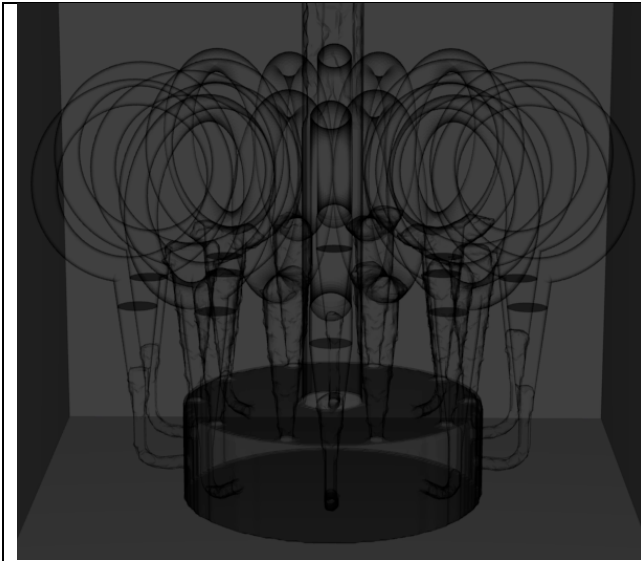


012 - Plenum With Ten Rings



013 - Rings on Top and Side of Plenum

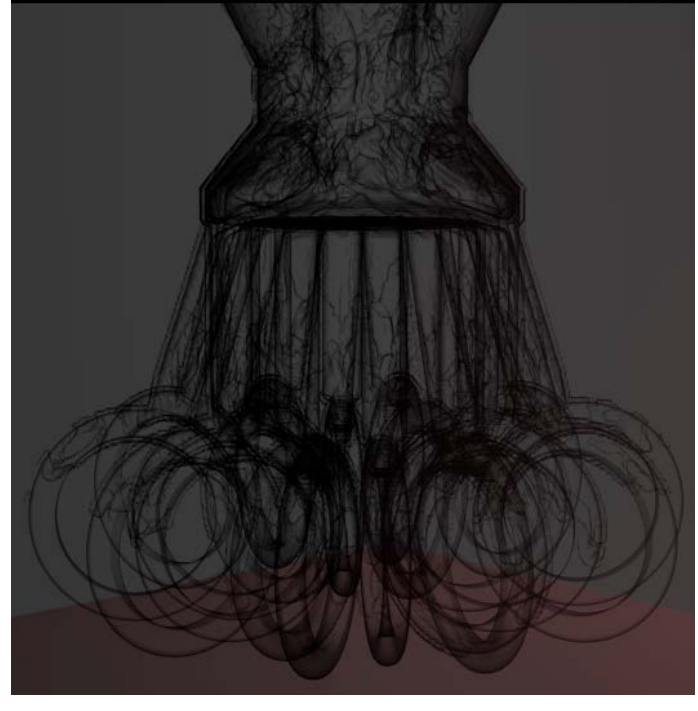
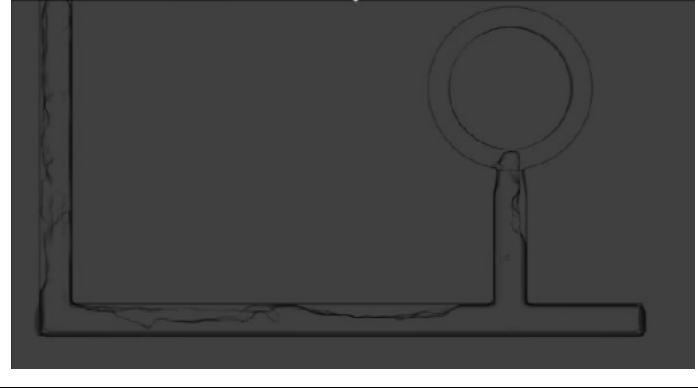

	<p>014 - Short Plenum (0p3cm)</p>
	<p>015 - Very Short Plenum (0p2cm)</p>

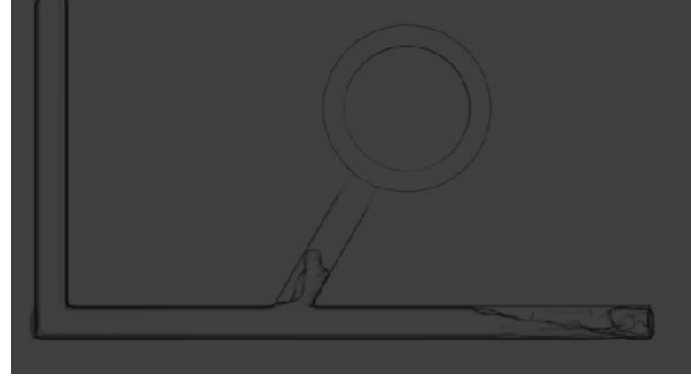
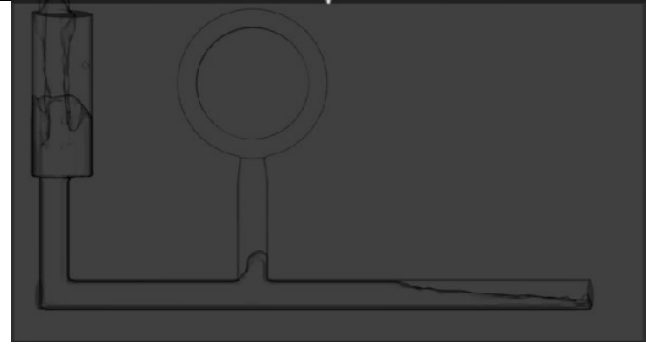
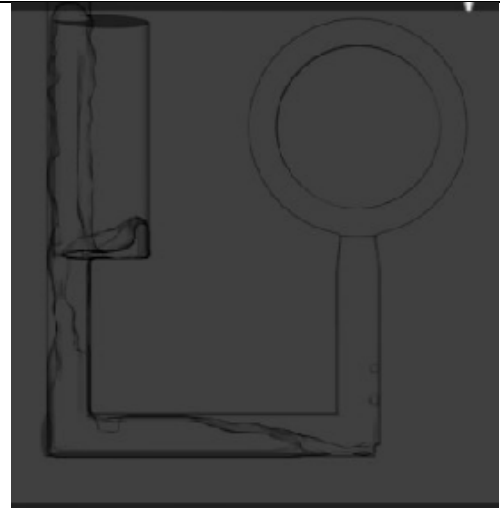


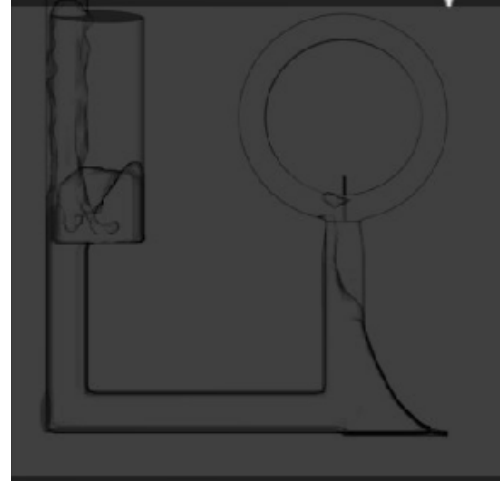
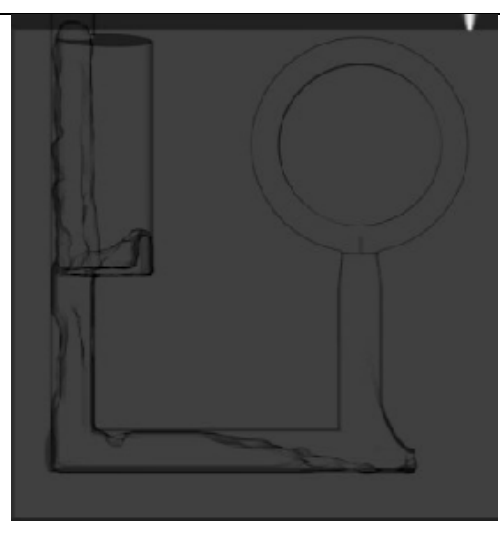
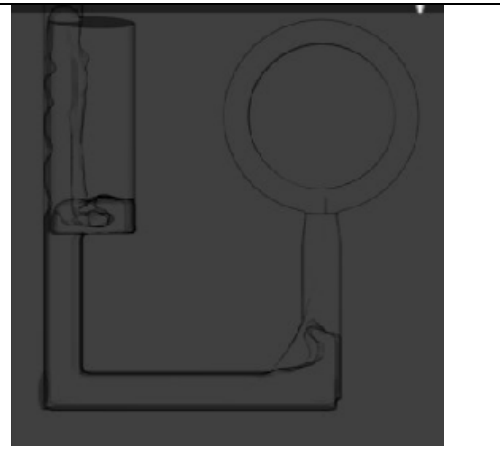
016 - Rings Top and Side
0p25 in dia sprue
0p4 in tall plenum

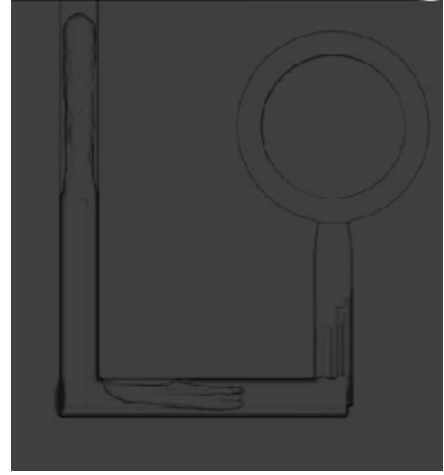
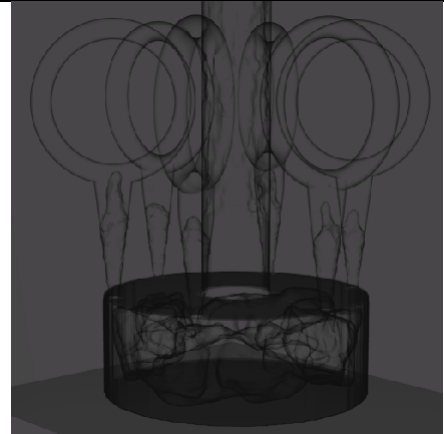
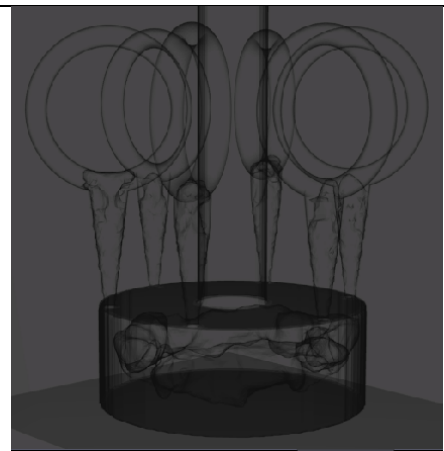


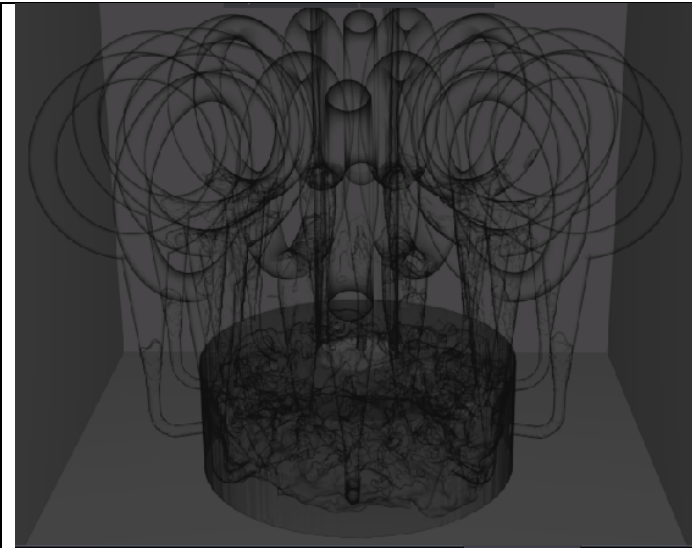
017 - Triangle Cross
Section Pipes

	<p>100_benchmark</p>
	<p>101_distance_to_ring</p>
	<p>102_squared_zigzag</p>

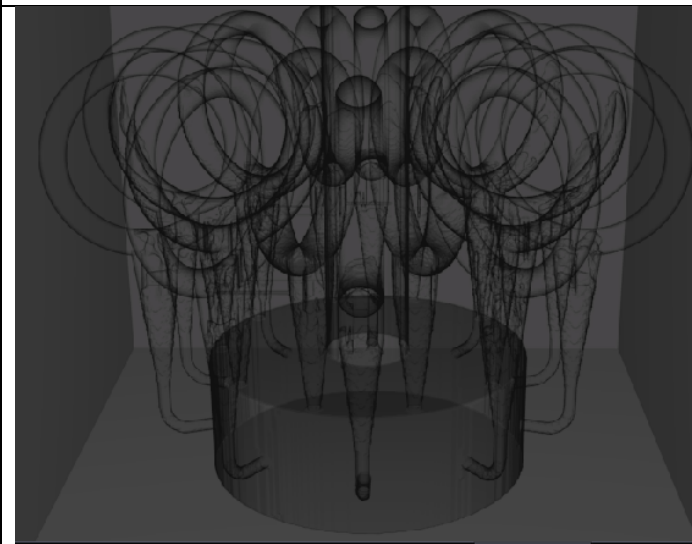
	103_angle of ring
	104_buffer
	105_buffer without tail

 A 3D CAD model of a mechanical part, labeled '106_with fin'. The part consists of a vertical cylindrical section on the left, a horizontal base, and a vertical stem on the right. The stem is topped with a circular flange. A thin, curved fin extends from the bottom of the stem. The model is shown in a dark gray color against a black background.		106_with fin
 A 3D CAD model of a mechanical part, labeled '107_base and fin'. The part is similar to the one in the first row, but the fin is more pronounced and has a different shape. The model is shown in a dark gray color against a black background.		107_base and fin
 A 3D CAD model of a mechanical part, labeled '108_smoothened corner'. The part is similar to the one in the first row, but the corner where the base meets the stem is smoothed. The model is shown in a dark gray color against a black background.		108_smoothened corner

		109_screen
		110_6 rings raw
		111_6 rings_screen



112_Plenum with Rings on Top and Side



113_Plenum with Rings on Top and Side_with screen

114_Final Design